Distinct effects of tubulin isotype mutations on neurite growth in *Caenorhabditis elegans*

Chaogu Zheng[*,†], Margarete Diaz-Cuadros[*,†], Susan Laura Jao[*], Ken C.Q. Nguyen[‡], David H. Hall[‡], and Martin Chalfie[*]

[*] Department of Biological Sciences, Columbia University, New York, New York, 10027, U.S.A.
[‡] Department of Neuroscience, Albert Einstein College of Medicine, Bronx, NY 10461, U.S.A.
[†] These authors contributed equally to the work.

Running title: Tubulin mutations and neurite growth

Key words: Microtubules, tubulins, Neurite growth, Touch receptor neurons, *Caenorhabditis elegans*

Correspondence:

Martin Chalfie
Department of Biological Sciences
1012 Fairchild, MC#2446
Columbia University
1212 Amsterdam Avenue
New York, NY 10027
Phone: 212-854-8870
Fax: 212-865-8246
Email: mc21@columbia.edu.

Abstract

Tubulins, the building block of microtubules (MTs), play a critical role in both supporting and regulating neurite growth. Eukaryotic genomes contain multiple α and β tubulin isotypes, and their dominant missense mutations cause a wide range of neurodevelopmental defects in humans. Thus, identifying the specific functions of each tubulin isotype and evaluating how particular mutations would change those functions during neuronal morphogenesis is fundamental for understanding MT functions in the nervous system. Using the *C. elegans* touch receptor neurons (TRNs), we analyzed the effects of 67 missense mutations in the *mec-12*/α-tubulin and *mec-7*/β-tubulin genes on neurite growth. Three types of mutations emerged: 1) loss-of-function mutations, which are found throughout the molecule and cause mild defects in neurite growth; 2) antimorphic mutations, which map to the GTP binding site and intradimer and interdimer interaction interfaces and significantly reduced MT stability, causing severe defects in the growth of all TRN neurites; and 3) neomorphic mutations, which map to the exterior surface and increased MT stability, causing ectopic neurite growth. Such structure-function analysis revealed a causal relationship between tubulin structure and interactions and MT stability, which in turn affects neuronal morphogenesis. Importantly, we engineered several disease-associated human tubulin mutations into *C. elegans* genes and examine their impact on neuronal development at cellular level. We also discovered a MT-destabilizing α-tubulin isotype TBA-7, whose loss led to the formation of hyperstable MTs and the generation of ectopic neurites; the lack of potential sites for polyamination and polyglutamination on TBA-7 may be responsible for this destabilization.

Introduction

Microtubules (MTs) play important roles in many aspects of neurite development, including the formation, extension, guidance, and maintenance of neurites (reviewed in DENT *et al.* 2011; PROKOP 2013; SAINATH AND GALLO 2015). The "search and capture" model (MITCHISON AND KIRSCHNER 1984) suggests that the dynamic instability of MTs allows them to explore the growth cone periphery until they are captured by stabilized actin filaments or membrane receptors enriched at the side of the growth cone responding to a guidance cue (TANAKA *et al.* 1995; CHALLACOMBE *et al.* 1996; SCHAEFER *et al.* 2008; QU *et al.* 2013). This capture transiently stabilizes MTs against catastrophe and enables MT elongation in the direction that the growth cone has turned. In addition to providing physical support for the neurite growth that follows the changes in actin dynamics, MTs also play an instructive role for neurite guidance. Since local application of the MT-stabilizing drug paclitaxel (also known as taxol) induced growth cone attraction and of the MT-destabilizing drug nocodazole induced repulsion (BUCK AND ZHENG 2002), signals that act by altering MT stability appear to directly initiate growth cone turning. Indeed, the guidance molecule Wnt can induce growth cone remodeling by changing the organization of MT structure through the inactivation of MT-plus end binding protein Adenomatous Polyposis Coli (PURRO *et al.* 2008). These results indicate that the regulation of MT dynamics is crucial for neurite growth and guidance, but how MT stability is controlled either locally at specific sites of the growth cone or globally in the entire neuron is not well understood.

As the building blocks of MTs, α- and β-tubulins are crucial determinants of MT stability. Eukaryotic genomes contain multiple tubulin genes encoding different isotypes (SULLIVAN 1988; MCKEAN *et al.* 2001) that are expressed in spatially and temporally distinct patterns (LEANDRO-

GARCIA *et al.* 2010). Different tubulin isotypes confer specific dynamic properties on MTs in tubulin polymerization assays *in vitro* (PANDA *et al.* 1994) and are not functionally equivalent *in vivo* in Drosophila (HOYLE AND RAFF 1990) or in single-celled organisms, such as *Tetrahymena thermophile* (PUCCIARELLI *et al.* 2012). These observations support the "multi-tubulin hypothesis," which proposes that distinct tubulin isotypes impart specific properties onto MTs, so they can perform particular cellular functions (FULTON AND SIMPSON 1976; CLEVELAND 1987). Moreover, tubulins also undergo a range of complex post-translational modification, which affect the dynamics of MTs and their interaction with other proteins (reviewed by SONG AND BRADY 2015). In neurons specifically, stable axonal MTs are more detyrosinated, acetylated, and glutamylated, whereas the dynamic MTs in the growth cone are more tyrosinated (LIAO AND GUNDERSEN 1998; KONISHI AND SETOU 2009). Tubulin isotypes and modifications at the C-terminal tail also control the velocity and processivity of MT motor proteins and microtubule depolymerization rates *in vitro* (SIRAJUDDIN *et al.* 2014). Therefore, post-translational modifications on different tubulins by a set of enzymes may generate a "tubulin code" that can be read by microtubule-associated proteins (MAPs), which regulate the organization of MTs and their interaction with other cellular components (VERHEY AND GAERTIG 2007; YU *et al.* 2015).

The clinical importance of tubulin genes in the development of the nervous system has been highlighted by the recent finding that patients carrying mutations in α- and β- tubulin genes showed microcephaly, lissencephaly, pachygyria, and other cortical malformations, as well as a range of axon guidance defects, including agenesis or hypoplasia of the corpus callosum, internal capsule, commissural fibers, and corticospinal tracts, depending on the mutations (TISCHFIELD *et al.* 2011). So far, based on three summaries (BAHI-BUISSON *et al.* 2014; LIU AND DWYER 2014; CHAKRABORTI *et al.* 2016), 60 point mutations in α-tubulin genes (51 in TUBA1A, 1 in

TUBA3E, and 8 in TUBA4A), one splicing-affecting intronic deletion in TUBA8, 48 point mutations in β-tubulin genes (2 in TUBB2A, 24 in TUBB2B, 19 in TUBB3, and 3 in TUBB5), and one exonic deletion in TUBB2B are known to cause tubulin-related neurological disorders in heterozygous carriers (Table S4); all mutations, except for the TUBA8 deletion, appear to have dominant-negative effects. Although mutated residues are found throughout the molecules, many are found in region predicted to mediate either GTP binding, heterodimer stability, inter-dimer interaction, or association with motor proteins and other MAPs (TISCHFIELD *et al.* 2011). Despite some *in vitro* studies on the effects of the mutations on tubulin folding, heterodimer assembly, and MT growth (JAGLIN *et al.* 2009; TIAN *et al.* 2010; TISCHFIELD *et al.* 2010), very few *in vivo* studies can systematically test how these different tubulin mutations impact axon guidance and extension in living organisms. Moreover, the complexity of the mammalian nerve system makes the analysis of the developmental consequences of these tubulin mutations very difficult.

Here, we use the morphologically simple and well-defined touch receptor neurons (TRNs) in the nematode *Caenorhabditis elegans* to model the effects of tubulin mutations on neurite growth. By analyzing a large collection of missense mutations in several tubulin genes, we found that these mutations caused three morphologically distinct defects in TRN neurite outgrowth: 1) the shortening of all TRN neurites; 2) the specific shortening of posteriorly-directed neurites; and 3) the production of ectopic posteriorly-directed neurites. The structural location of the mutated residue correlated with the resulting phenotype. Many tubulin mutations characterized in our study affect the same amino acid residue or region as the disease-causing mutations. We generated several such human mutations in *C. elegans* tubulin genes through genome editing and found that they also caused distinct neurite growth defects that fall into the above categories. Thus, our system may be used to understand the different effects of the clinically identified

184 tubulin mutations and to facilitate their classification. Moreover, we found that null mutations in
185 two α-tubulin genes led to very different phenotypes, supporting the hypothesis that tubulin
186 isotypes perform specific and often non-overlapping roles in neurite development.

187 **Results**

188 **A genetic screen for TRN neurite growth defects**

189 The six mechanosensory TRNs (ALML/R, PLML/R, AVM, and PVM) in *C. elegans* are
190 a useful model to study axonal outgrowth and guidance because of their well-defined
191 morphology (CHALFIE AND SULSTON 1981). The ALM and PLM neurons are two pairs of
192 embryonically derived, bilaterally symmetric cells, whereas the AVM and PVM neurons arise
193 from postembryonic lineages. All six neurons have a long anteriorly-directed neurite (AN); in
194 addition, the two PLM neurons have a posteriorly-directed neurite (PN), making them bipolar.
195 Except in PVM, the AN branches at its distal end; we refer to this branch as the synaptic branch.

196 Previous studies had identified several components needed for proper TRN outgrowth:
197 UNC-6/Netrin (HEDGECOCK *et al.* 1990), LIN-44/Wnt proteins (HILLIARD AND BARGMANN
198 2006), and a few other signaling molecules (DU AND CHALFIE 2001). To systematically search
199 for genes involved in the regulation of neurite growth, we performed an extensive genetic screen
200 to isolate mutants with defects in TRN neurite extension. We mutagenized a strain (TU4069)
201 carrying the *uIs134* transgene, which allows RFP expression from the TRN-specific *mec-17*
202 promoter, and screened the progeny of individual F1 animals representing 20,200 haploid
203 genomes. Although we focused on isolating mutants whose TRNs had morphological defects, we
204 also obtained mutants with abnormal numbers of fluorescently labeled cells. This screen yielded
205 80 mutants. We identified the phenotype-causing mutations for 62 mutants; the remaining
206 mutants either were of low penetrance (7) or did not yield a confirmable mutation (11). The

characterized mutations represented 26 genes. Mutations in 8 genes caused the loss of TRN marker expression or its expression in extra cells, and mutations in 2 genes specifically affected the development of the postembryonic AVM and PVM neurons (Table S1); most of these mutant phenotypes were previous described and thus are not discussed here. Mutations in the remaining 16 genes resulted in various TRN neurite extension defects, which were organized into seven phenotypic categories (A-G, Table S2). This screen is likely to be near saturation because 1) the number of haploid genomes examined is 10 times the reciprocal of the average mutation rate (5×10^{-4}) for null alleles (BRENNER 1974); and 2) nine of the ten genes represented by multiple alleles had three or more alleles.

The 16 genes whose products regulate neurite outgrowth and guidance (Table S2) encode proteins that affect either extracellular signaling to the TRNs, intracellular signaling, or effectors that are directly involved in cytoskeleton rearrangement and growth cone movement. Molecules affecting extracellular signaling include the guidance protein LIN-44/Wnt and its receptor LIN-17/Frizzled, and three proteins, UNC-23, MUA-3, and SUP-26 not acting within the TRNs. PLM neurites in *lin-44* and *lin-17* mutants failed to navigate towards the anterior (category D) because of the repellent activity of the Wnt signal (HILLIARD AND BARGMANN 2006; ZHENG *et al.* 2015a). *unc-23* (category G) and *mua-3* (category B) are only expressed in muscle cells (BERCHER *et al.* 2001; PAPSDORF *et al.* 2014), and their mutant phenotypes could not rescued by TRN-specific expression of the wild-type gene. Similarly, mutations in *sup-26* (category B), which encodes a RNA-binding protein and is expressed in most somatic cells (MAPES *et al.* 2010), could not be rescued by TRN-specific expression of the wild-type gene. We have not investigated how these molecules affect neurite outgrowth and guidance in a non-cell autonomous manner.

Genes encoding molecules that are presumably involved with intracellular signaling include *unc-51*, *mec-15*, *dsh-1*, *egl-5*, *unc-73*, and *tiam-1*. *unc-51* encodes a serine/threonine-protein kinase; mutation of *unc-51* caused general outgrowth and guidance defects (category A; DU AND CHALFIE 2001). *mec-15*, which is needed for touch sensitivity (Au and Chalfie, 1989), encodes a F-box protein with WD repeats and so is likely to mediate ubiquitination and protein degradation (category E; BOUNOUTAS *et al.* 2009b). Mutation of *mec-15* caused shortening of both PLM neurites. We previously reported that DSH-1/Dishevelled (category B) negatively modulates the activity of Wnt signaling to allow posterior outgrowth against the Wnt gradients (ZHENG *et al.* 2015a) and that *egl-5* (category B), which encodes a Abd-B-like Hox transcription factor, promotes PLM differentiation by inducing the growth of PLM-PN and at least one downstream effector (ZHENG *et al.* 2015b). We also identified guanine nucleotide exchange factors (GEFs) [UNC-73/Trio (category E) and TIAM-1 (category B)], which controls neurite extension towards the anterior and posterior, respectively (ZHENG *et al.* 2016).

In this study, we describe the role of the downstream effectors of directional neurite outgrowth, the presumed targets of extracellular and intracellular signaling: primarily tubulin isotypes (MEC-7/β-tubulin, MEC-12/α-tubulin, and TBA-7/α-tubulin) and kinesin motor proteins (KLP-7 and KLP-11). MEC-7 and MEC-12 are expressed at high levels in the TRNs (HAMELIN *et al.* 1992; MITANI *et al.* 1993), which contain large diameter (15-protofilament, 15-p) MTs instead of the typical 11-protofilament (11-p) MTs found in all other cells (CHALFIE AND THOMSON 1979; SAVAGE *et al.* 1994). Combining the alleles isolated in our screen, created through genome editing, and previously obtained by our lab (SAVAGE *et al.* 1994) and the million mutation project (THOMPSON *et al.* 2013), we collected in total 78 alleles representing 48

different missense mutations in *mec-7* and 19 in *mec-12* (Table 1) and found that these mutations led to various outgrowth defects (category A, B, and C defined in Table S2).

mec-7/β-tubulin, but not _mec-12_/α-tubulin, is needed to form 15-p MTs

Previous studies suggested that the α-tubulin MEC-12 and the β-tubulin MEC-7 form the TRN-specific 15-p MTs that assemble into bundles to fill up the TRN neurites and are required for the mechanosensory functions of TRNs (CHALFIE AND THOMSON 1979; CHALFIE AND AU 1989; SAVAGE *et al.* 1994; BOUNOUTAS *et al.* 2009a). We first examined the MT structures of the *mec-12(tm5083)* and *mec-7(ok2152)* deletion alleles using electron microscopy (EM; Figure 1A and S1). *mec-12* and *mec-7* knockout animals had on average 7 and 6 MTs, respectively, in a cross section of the ALM neurite compared to 31 MTs in the wild type animals (Figure 1B). MTs in *mec-12(tm5083)* animals had the same diameter as the 15-p MTs in the wild-type animals, whereas the diameter of MTs in *mec-7(ok2152)* animals was much smaller (16.6 nm; Figure 1). These results suggest that although the abundance of MTs is dependent on both MEC-12 and MEC-7, the formation of 15-p MTs requires MEC-7 but not MEC-12; other α-tubulin genes may compensate for the loss of MEC-12. In the absence of MEC-7, however, the 15-p MTs in TRNs are replaced by smaller, presumably 11-p, MTs.

The *mec-7* result is similar to our previous observations on *mec-7(e1506)* animals (the e1506 mutation alters the start codon and results in no detectable mec-7 mRNA; CHALFIE AND THOMSON 1982; SAVAGE *et al.* 1994). In contrast, the *mec-12* result was unexpected, because the *mec-12[(e1607* (G144S)*]* allele, which was regarded as the null allele in several previous studies (BOUNOUTAS *et al.* 2009a; BOUNOUTAS *et al.* 2011; HSU *et al.* 2014), had very few (~2) MTs, all of which had the small diameter (CHALFIE AND AU 1989; also this study). We found that *e1607* and several previously characterized missense alleles were in fact antimorphic (*anti*) gain-of-

function alleles and their phenotypes in neurite growth was also different from the *mec-12* loss-of-function (*lf*) mutants (see below).

Loss-of-function mutations in *mec-7*/β-tubulin but not *mec-12*/α-tubulin cause defects in posteriorly directed neurite growth

To test whether MEC-12 and MEC-7 were needed for neurite growth, we examined the outgrowth in animals with *mec-12* and *mec-7* null alleles. No defects in TRN outgrowth were found in animals mutant for four presumably null *mec-12* alleles [the knockout allele (*tm5083*) and three frameshift mutations (*u1026*, *u1027*, and *u1028*; Figure S1A)] (Figure 2). These results suggest that MTs made without MEC-12 can still respond normally to guidance cues and support neurite morphogenesis. Because *C. elegans* genome contains nine α-tubulin genes, other tubulin isotypes may compensate for the loss of MEC-12. One such candidate is TBA-7/α-tubulin, which is expressed and functions in TRNs (see below); however, *mec-12; tba-7* double mutants were still capable of forming and growing normal TRN neurites, suggesting further genetic redundancy.

Null mutations in *mec-7* (*ok2152*, *u156*, and *u440*; Figure S1B) only slightly affected the growth of anteriorly-directed neurites but markedly shortened the PLM-PN (Figure 2B). This result suggests that PLM-AN and PLM-PN, which arise at the same time in the embryo, have different tubulin requirements. Normally the PLM-AN extends anteriorly past the vulva to within 50 μm of ALM cell body. Lockhead et al. (2016) reported that the gap between the end of PLM and ALM cell body was wider in *mec-7 lf* mutants due to the shortening of the PLM-AN (LOCKHEAD *et al.* 2016). We also found a similar modest widening of the gap in *mec-7(ok2152)* animals, but 92% of the PLM-ANs still extended beyond the vulva (Figure 2B and D). Moreover, no shortening of the ALM-AN was seen. A more penetrant and striking defect, however, was the

297 fact that 78% of PLM-ANs in *mec-7(ok2152)* lacked a synaptic branch, which normally arises
298 posterior to the vulva (Figure 2A and S2). In our analysis, 12 missense mutations (Table 1),
299 including the newly isolated *u1020* (G34S) allele, caused a similar *mec-7* null phenotype.
300 The above results and EM data suggest that 1) the reduction of MT numbers in *mec-12 lf*
301 mutants does not affect neurite development; 2) the smaller, generic 11-p MTs in *mec-7 lf*
302 mutants are capable of supporting general neurite growth in TRNs; 3) the presence of 15-p MTs
303 is essential for the normal extension of PLM-PN.
304 In addition to neurite growth, MTs are important for many other functions in TRNs,
305 which were studied before using a few *mec-12* and *mec-7* missense alleles (BOUNOUTAS *et al.*
306 2009a; HSU *et al.* 2014). In this study, we systematically confirmed their phenotypes using the
307 knockout mutants and also compared the null alleles with *gf* alleles for those phenotypes (Figure
308 3). Deletion of either *mec-12* or *mec-7* resulted in touch insensitivity, defects in the localization
309 of pre-synaptic vesicles, and severe loss of MT acetylation, a mark for stable MTs. Since MEC-
310 12 is the only α-tubulin isotype that contains the acetylation site (lysine 40) in *C. elegans*, the
311 TRN-specific 15-p MTs are likely the only MTs that can be acetylated. The loss of *mec-7* and
312 *mec-12* also induced a global reduction in protein levels through a mechanism dependent on the
313 dual leucine zipper-bearing kinase DLK-1 (BOUNOUTAS *et al.* 2011). Interestingly, mutations in
314 *dlk-1* restored the normal protein expression in *mec-7* and *mec-12* null mutants but failed to
315 rescue the PLM-PN growth defects in *mec-7(ok2152)* animals (Figure 3D). Therefore, this PLM-
316 PN defect is most likely a direct effect of the loss of MEC-7 and not the result of secondary
317 changes in protein levels.
318 Several *mec-12* partial *lf* mutations affected only a subset of MT functions. *mec-12(e1605)*
319 animals carrying the H192Y missense mutation were defective in mechanosensation but had

retained normal 15-p MT structures, tubulin acetylation, axonal transport, protein levels, and neurite growth patterns (Figure S3; BOUNOUTAS *et al.* 2009a). Similarly, *mec-12* mutants carrying the *u63* (E415K) or *gm379* (G416E) alleles were partially touch-insensitive but kept the large dimeter MTs; however, these animals showed mistargeting of synaptic vesicles presumably because alterations in the EEGE (amino acid 414-417) motif increased affinity with the motor dynein (HSU *et al.* 2014). *u63* and *gm379* mutations also caused a slight decrease in tubulin acetylation and a partial reduction in protein production; *gm379* allele led to very mild defects in the growth of PLM-PN (Figure S3). These mutations may be useful in understanding some specific aspects of MT functions.

Antimorphic mutations in *mec-7*/β-tubulin led to severe, general defects in neurite outgrowth

We identified 19 strong *mec-7*(*anti*) gain-of-function missense mutations (Table 1) that caused severe shortening of all TRN neurites (Figure 2B); the ALM-AN did not reach the pharynx, the PLM-AN terminated before reaching the PVM cell body and the PLM-PN was shortened (Figure 2D). We also identified 4 weak *mec-7(anti)* mutants (Table 1), in which ALM-AN did not extend beyond the nerve ring and PLM-AN did not reach the vulva. All of these alleles, except the recessive *u430* (A97V) mutation, were either dominant or semi-dominant. Early studies of one of the dominant *mec-7* alleles, *e1343* (P171L), found that the mutants contained very few (2.8 ± 0.5 in a cross section) MTs (CHALFIE AND THOMSON 1982), which suggests that the *anti* mutations may block MT polymerization and thereby cause the severe neurite outgrowth defects. In fact, when compared to the *mec-7(ok2152)* null allele, these *anti* mutations caused stronger defects not only in neurite outgrowth, but also in touch sensitivity, synaptic vesicle transport, tubulin acetylation, and protein expression levels (Figure 3).

343 Mutations in *dlk-1* could block the reduction in global expression but failed to rescue the neurite
344 growth defects (Figure 3D).

345 The amino acid residues mutated in the antimorphs are located in three regions on the
346 structure of an αβ tubulin dimer determined by electron crystallography (NOGALES *et al.* 1998):
347 1) the GTP/GDP binding pocket, 2) the intradimer interface, and 3) the lateral or longitudinal
348 interdimer interface. All of which are important for tubulin polymerization. For example, *u430*
349 (A97V), *u911* (P171S), *u957* (P171L), and *u262* (N226Y) mutations alter amino acids in direct
350 contact with the GTP molecule, and *u48* (S176F) and *u449* (V179A) change amino acids in the
351 B5 (the fifth β-strand)-to-H5 (the fifth α-helix) loop, which is crucial for forming the GTP/GDP
352 binding pocket (Figure 4C). Two other mutations *u445* (M300V) and *u98* (M300T) substitute
353 M300, which is located in a loop near the GTP binding site and may participate in positioning
354 H7 (the seventh α-helix) with its critical N226, and thus indirectly affect GTP binding.

355 The second group of mutated residues in *mec-7(anti)* alleles is located in the intradimer
356 interface, where β-tubulin makes contact with α-tubulin to form the heterodimer (red residues in
357 Figure 4D). *u283* (P243L), *u958* (G244S), *n434* (N247I), and *u162* (D249N) mutations all affect
358 the residues on the H7-to-H8 loop, which interacts extensively with residues on H1 and H2 of α-
359 tubulin. Two other dominant mutations *gk286000* (A314V) and *u955* (A352T) changed residues
360 that located on B8 and B9, respectively, which are physically adjacent to the H7-to-H8 loop at
361 the interface. In addition, two prolines mutations, *u910* (P357L) and *u956* (P358L) possibly
362 disrupted the B9-to-B10 loop (a.a. 356-361) critical for the positioning of B9.

363 The third group of *mec-7(anti)* alleles include *e1527* (V286D), *u18* (A393T), and
364 *gk285997* (A393V), which affect residues involved in the lateral (V286) and longitudinal (A393)

365 interdimer interaction between one α/β-tubulin heterodimer and the neighboring one on the MTs.
366 These mutations may interfere with the interaction between tubulin dimers.

367 Overall, the above β-tubulin antimorphs likely act as dominant-negative mutants by
368 forming a poisonous α/β dimer, whose incorporation into MTs could terminate MT
369 polymerization and induce instability; the mutated β-tubulin either cannot properly bind to GTP
370 (the first group) or form misshaped α/β heterodimers that block the growing end of MTs (the
371 second group) or disrupt the stacking of tubulin dimers (the third group). Therefore, changes in
372 tubulin structure led to compromised MT elongation, which caused severe defects in neurite
373 outgrowth, highlighting the importance of functional MTs in neuronal morphogenesis.

374 **Antimorphic mutations in *mec-12*/α-tubulin led to specific defects in posteriorly directed**
375 **neurite growth**

376 Similar to the *mec-7(anti)* mutations, we identified 5 *mec-12(anti)* mutations that also
377 mapped to the GTP binding pocket [*u76* (D69N), *u950* (S140F), and *u1021* (G144S); labeled in
378 red in Figure 4B], the intradimer interface [*u1016* (E97K); Figure 4D], or the interdimer
379 interface [*u1019* (G354E)]. However, these *mec-12* antimorphs are mostly recessive, except for
380 *u1019*, and did not cause strong, general defects in TRN neurite outgrowth. Instead, these
381 mutations led to the specific shortening of PLM-PN, similar to the defects observed in *mec-7* null
382 animals. Electron microscopy studies revealed that the *mec-12(anti)* mutants have very few small
383 diameter MTs (*e.g.* ALM neurons in *u1021* animals had on average 2.7 MTs in a cross section
384 and 15% of the 72 sections examined had no MTs; the diameter of MTs was 17.9 nm on average;
385 Figure 1B). Therefore, *mec-12(anti)* mutations have distinct phenotypes from the *lf* alleles,
386 which retained 15-p MTs and had no defects in neurite formation. The *e1607* (G144S) allele,
387 which was previously thought to be a null allele, had the same molecular lesion as antimorph

388 *u1021* and caused the shortening of PLM-PN (Figure 2E) and the loss of 15-p MTs (CHALFIE
389 AND AU 1989); these results further confirm that *e1607* should not be regarded as a *lf* allele.
390 In addition, the *mec-12* antimorphs also resulted in touch insensitivity, reduction in
391 tubulin acetylation, synaptic vesicle mistargeting, and decrease in TRN protein levels; these
392 phenotypes were much stronger than the phenotypes of *mec-12* null alleles and were comparable
393 to those produced by *mec-7* null mutations but not *mec-7 anti* mutations (Figure 3). One possible
394 explanation for this phenotype is that MEC-12/α-tubulin preferentially or exclusively binds to
395 MEC-7/β-tubulin, and MEC-12 mutant proteins could only sequester and disable MEC-7 but not
396 other β-tubulin isotypes. As a result, either *anti* mutations in *mec-12* or *lf* mutations in *mec-7*
397 could eliminate the specialized, large diameter, stable MTs that require the MEC-12/MEC-7
398 heterodimer, but neurite growth could still be supported by regular MTs formed with other α-
399 and β-tubulin isotypes. Consistent with this hypothesis, *mec-7(lf); mec-12(anti)* double mutants
400 did not show additive effects with regards to the neurite growth defects compared to either single
401 mutant (Figure 2E).
402 The specific shortening of PLM-PN in *mec-7* null mutants and *mec-12* antimorphs may
403 be caused by higher sensitivity of the posteriorly neurites to changes in microtubule stability
404 compared to the anteriorly directed neurites. The normal 15-p MTs exist in great numbers and
405 form bundles, which may provide stronger support for neurite growth than the few 11-p MTs
406 found in the mutants. In fact, treatment with the MT-destabilizing drug colchicine (1mM) led to
407 a similar shortening of the PLM-PN, phenocopying these mutations (Figure S4).
408 **Neomorphic mutations in *mec-7* and *mec-12* resulted in the growth of ectopic neurites**
409 A third category of *mec-7*/β-tubulin mutations resulted in novel phenotypes, different
410 from the effects of either *mec-7 lf* or *anti* mutations; these neomorphic (*neo*) alleles caused the

411 growth of an extra posteriorly directed neurite in ALM neurons, as well as the overextension of
412 the PLM-PN. Three such alleles [*u170* (E407K), *u278* (C303Y), and *ky852* (P220S)] were
413 previously reported (SAVAGE *et al.* 1994; KIRSZENBLAT *et al.* 2013), and three more [*gk895768*
414 (T149I), *gk286003* (R162Q), and *u1017* (L377F)] were identified in this study. L377 and E407
415 are located on the H11 and H12 helices, respectively, both of which are on the exterior side of
416 MTs and may, therefore, bind motor proteins and other MAPs (Figure 4E). R162 on the H4-to-
417 B5 loop and C303 on the H9-to-B8 loop are also exposed on the MT surface, whereas T149 and
418 P220 are located inside the tubulin structure and may be important for the folding of the protein.
419 Among these six alleles, *u278* (C303Y) produced the strongest phenotype; the ectopic posterior
420 neurite of ALM neurons often extended posteriorly to the PLM cell body (Figure 2B).
421 Interestingly, the C303S mutation in allele *gk286001* did not lead to similar excessive growth
422 (Table 1), suggesting that tyrosine's bulky phenolic ring may be responsible for the phenotype.
423 We also found four *mec-12*/α-tubulin *neo* alleles [*gk170196* (P32S), *gk915672* (E196K),
424 *u917* (V260I), *gk515972* (V323I)], which generated similar but less severe phenotypes than the
425 *mec-7(neo)* alleles, since the ectopic ALM-PN was shorter in the *mec-12* mutants than in the
426 *mec-7* mutants (Figure 2F). This observation supports the notion that MEC-12 may be less
427 critical than MEC-7 in controlling MT dynamics and neurite growth. E196 and V260 are located
428 on loops on the exterior surface, whereas P32 and V323 may be involved in protein folding
429 (Figure 4F).
430 The production of the ectopic ALM-PN requires both *mec-7* and *mec-12*. The *mec-12*
431 null alleles suppressed the ALM posterior outgrowth in *mec-7(neo)* mutants, and *mec-7 lf*
432 mutation similarly suppressed the effect of *mec-12(neo)* alleles (Figure 6A). We also conducted a
433 suppressor screen to search for mutations that can suppress the strong phenotype of ALM-PN

growth in *mec-7(u278 neo)* mutants. After screening 16,000 haploid genomes, we isolated three suppressors: 1) an intragenic mutation in *mec-7* [*u1040* (G98E)], 2) a *lf* mutation in *mec-12* [*u1041* (G246E)], and 3) a *lf* mutation in *mec-15* [*u1042* (R27*)]. The identification of *mec-7* and *mec-12* mutations as suppressors suggests that the incorporation of the MEC-7/MEC-12 heterodimers into the MTs is required for the generation of the excessive neurite; the role of *mec-15*, which codes for an F-box protein with WD repeats, is described below.

Neomorphic mutations in *mec-7* and *mec-12* increase MT stability

These neomorphic tubulin mutations appeared to increase the stability of MTs, as first suggested by KIRSZENBLAT *et al.* (2013) for *mec-7.* Supporting this hypothesis, pharmacological stabilization of MTs with paclitaxel induced the growth of ALM-PN, although at a low frequency (KIRSZENBLAT *et al.* 2013), and destabilizing MTs with colchicine can partially suppress this ectopic growth in *mec-7(ky852)* mutants (KIRSZENBLAT *et al.* 2013) and in *mec-7(u278)*, *mec-7(u1017)*, and *mec-12(u917)* animals (Figure 6A). Moreover, these mutants also showed increased tubulin acetylation (Figure 3C), an indication of stable MTs (SONG AND BRADY 2015). *mec-7(u278)* and *mec-7(u170)* mutants had large diameter MTs (slightly larger than in wild-type cells), but fewer of them (Figure 1B). Moreover, the MT bundles in the mutants are more closely spaced than the wild type and are not surrounded by the electron-lucent region seen in the wild type (SAVAGE *et al.* 1994); we quantified these differences by showing that the distance between two closest center points of MTs is smaller in *mec-7* neomorph compared to the wild type and that MTs occupied a bigger proportion of the cross-sectional area of the neurite in the mutants (Figure 1B). In fact, the TRN neurite in these mutants is about 50% thinner than the wild type animals. The observation that tightly packed 15-p MT bundles filled up most of the space in the TRN neurites is consistent with increased MT stability, which

457 presumably allowed the excessive neurite growth towards the posterior, overcoming the normal
458 inhibition of this growth in the wild-type ALM neurons.

459 Another line of evidence indicating higher stability of MTs in *mec-7* and *mec-12*
460 neomorphs came from their increased resistance to colchicine. This MT-destabilizing drug
461 caused the similar level of reduction in both touch insensitivity and PLM-PN length at a higher
462 concentration in the *neo* mutants than in the wild type animals (Figure S4). Because the majority
463 of the altered residues in the *neo* alleles are located on the exterior surface of MTs, these
464 mutations may interfere with the binding of motor proteins or MAPs to the MTs and therefore
465 cause changes in MT stability.

466 The *mec-7* and *mec-12 neo* alleles also caused some of the same phenotypes that *lf*
467 mutations do, such as touch insensitivity, synaptic vesicle mistargeting, and reduced TRN
468 protein levels, suggesting that an optimal stability of MTs is needed for their proper functions.
469 Furthermore, the fact that these phenotypes can occur in conjunction with either impaired (in *anti*
470 mutants) or excessive (in *neo* mutants) neurite growth support to the hypothesis that the role of
471 MTs in regulating neurite development is genetically separable from other MT functions.

472 **Modeling the effects of tubulin mutations using the TRN neurites**

473 Our genetic analysis shows that missense mutations in tubulin genes can have distinct
474 effects on MT stability and neurite growth pattern, and those different phenotypes appear to
475 correlate with the positions of the altered residues in the tubulin structure. Such structure-
476 function analyses were carried out before for yeast α-tubulin TUB1 and for Drosophila testis-
477 specific β-tubulin βTub85D (FACKENTHAL *et al.* 1995; RICHARDS *et al.* 2000) but not for
478 tubulins in the nervous system. Moreover, recent discovery of over a hundred missense
479 mutations in tubulin genes in patients with a range of neurological disorders prompted us to

examine the cellular impact of specific tubulin mutations on neurons. Combining the convenience of genome editing in *C. elegans* and the ease of observing TRN morphology as the readout of MT stability and neurite growth, we could systematically study the effects of those human tubulin mutations. To provide proof of concept, we generated five clinically observed β-tubulin mutations (S172P, P173L, A302T, P380S, and E410K) in *mec-7* through CRISPR/Cas9-mediated gene editing (Materials and Methods; Figure 5A) and found that these mutations indeed caused distinct phenotypes on TRN morphogenesis.

S172P and P173L mutations in human TUBB3 were found in heterozygous patients with microcephaly, polymicrogyria, cortical dysplasia, and agenesis of the corpus callosum, which are defects in neuronal migration and axon growth (JAGLIN *et al.* 2009; POIRIER *et al.* 2010; BAHI-BUISSON *et al.* 2014). *In vitro* studies found that tubulin heterodimer containing the β-tubulin S172P mutant could not be incorporated into MTs (JAGLIN *et al.* 2009), indicating that the mutated protein is nonfunctional. Consistent with these findings, the *u1056* (S172P) mutation of *mec-7* led to a recessive *loss-of-function* Mec-7 phenotype in the TRNs, which showed significantly shortened PLM-PN and slightly shortened PLM-AN with branching defects (Figure 5B, i). Surprisingly, the *u1057* (P173L) allele did not cause any TRN morphological or functional defects (Figure 5B, ii). The difference between the mutant phenotypes in humans and worms is puzzling, since both S172 and P173 are located on the GTP binding B5-to-H5 loop (Figure 4C), which is identical in *C. elegans* MEC-7 and human TUBB3 (Figure S5). Perhaps the differences arise from differences in MT structure and organization: the *C. elegans* TRNs have 15-p MTs that are bundled, whereas human neurons have 13-p MTs that are not bundled. In fact, when 15-p MTs were converted to 13-p MTs and the bundle was disrupted in *mec-17* (α-tubulin acetyl-transferase) mutants (TOPALIDOU *et al.* 2012), both MEC-7 S172P and P173L

503 mutations led to decreased MT stability and the loss of ALM-PN (Figure 5B, iii). This result
504 suggests that P173L mutation indeed compromises MT stability in TRNs under sensitized
505 conditions.

506 Heterozygous A302T and R380C mutations in human TUBB3, which affect residues on
507 the external surface of the MTs, were associated with moderate congenital fibrosis of the
508 extraocular muscles 3 (CEFOM3), anterior commissure hypoplasia, and corpus callosum
509 hypoplasia. Mutation of A302 and R380 in yeast led to the formation of highly stable, benomyl-
510 resistant MTs (TISCHFIELD *et al.* 2010). Consistent with these observations, we found that the
511 same mutations of MEC-7 produced a *neo* phenotype (the generation of an ectopic ALM-PN;
512 Figure 5B, iv and v).

513 TUBB3 E410K mutation was also found in patients with severe CEFOM3 and hypoplasia
514 of anterior commissure and corpus callosum, but these patients also suffer from facial weakness
515 and progressive axonal sensorimotor polyneuropathy (TISCHFIELD *et al.* 2010). In yeast, MTs
516 containing β-tubulin with the E410K substitution were less stable and less resistant to benomyl
517 and had markedly decreased plus-end accumulation of kinesin-like motor proteins, compared to
518 MTs with A302T and R380C mutations (TISCHFIELD *et al.* 2010). In *C. elegans*, MEC-7(E410K)
519 produced a distinct neurite growth phenotype: ALM-AN and PLM-AN, but not PLM-PN were
520 significantly shortened, which indicates reduced MT stability; but the PLM-PN was not affected,
521 making the phenotype also different from that of the *mec-7* antimorphs, which cause general
522 defects in MT polymerization (Figure 5B, vi). Since E410 is also exposed to the exterior of MTs
523 like A302 and R380 (Figure 4E), these results suggest that the cellular impact of the missense
524 mutations would depend on the specific amino acid change instead of the location of the affected
525 residues alone.

The loss of *tba-7*/α-tubulin also caused excessive posterior neurite growth

C. elegans genome contains nine α-tubulin genes (*mec-12*, *tba-1*, *tba-2*, and *tba-4* through *tba-9*) and six β-tubulin genes (*ben-1*, *mec-7*, *tbb-1*, *tbb-2*, *tbb-4*, and *tbb-6*). Our screen yielded mutants in only three of these genes: *mec-7*, *mec-12*, and *tba-7*. The missense *tba-7* allele *u1015* (G92D) caused the growth of an ectopic ALM posterior neurite, resembling the phenotype of *mec-7* and *mec-12 neo* alleles. This *tba-7* allele is likely a *lf* allele, because it failed to complement with *gk787939* (Q230*), which is presumably a null and produced similar phenotype as *u1015* (Figure S1C). We also examined mutants of other tubulin isotypes, and did not find morphological defects in the TRNs (we did not test for redundancy among the genes; Table S3).

tba-7 was expressed in the TRNs, and the excessive growth phenotype of *tba-7(u1015)* could be rescued by expressing *tba-7(+)* from the TRN-specific *mec-17* promoter, indicating that TBA-7 acts cell-autonomously in the TRNs (Figure S6). *tba-7 lf* mutants did not exhibit touch insensitivity, synaptic vesicle mistargeting, or reduced protein levels, suggesting that the general function of TRN MTs was not affected and that the primary function of TBA-7 is to regulate neurite growth (Figure S7). We hypothesized that the loss of TBA-7 led to the formation of hyperstable MTs, similar to the *mec-7* and *mec-12 neo* mutations. Supporting this hypothesis, electron microscopy studies revealed that, like *mec-7(neo)* mutants, *tba-7(u1015)* animals retained the large diameter 15-p MTs and have closely packed MT bundles, which occupied a larger-than-normal area of a neurite cross-section (Figure 1). *tba-7 lf* mutants also retained normal tubulin acetylation levels (Figure S7C) and had increased resistance to colchicine (Figure S4), which confirmed the presence of stable MTs. Treatment with 1 mM colchicine fully

548 suppressed in the growth of ALM-PN in *tba-7(u1015)* animals, and either *lf* or *gf* mutations in
549 *mec-7* or *mec-12* could do so as well (Figure 6A).

550 The amino acids sequences of α-tubulin TBA-7 and MEC-12 are 82% identical and 94%
551 similar; they mainly differ in a N-terminal region and the C-terminal tail (Figure 6C). Domain
552 swapping experiments showed that changing L31 of TBA-7 to Q found in MEC-12 or replacing
553 the C-terminal DANDNGD (a.a. 435-441 in TBA-7) sequence with MEDNGEEG (a.a. 440-447
554 in MEC-12) partially impaired the function of TBA-7 proteins to restrict excessive neurite
555 growth; and TBA-7 proteins with both L31Q mutation and the C-terminal replacement
556 completely lost the ability to rescue the *tba-7 lf* phenotype (Figure 6D). Q31 in MEC-12 is a
557 potential site for polyamination (SONG *et al.* 2013) and E445 of the GEE motif (a.a. 444-446 in
558 MEC-12, but absent in TBA-7) is a target for polyglutamination (EDDE *et al.* 1990). Post-
559 translational modifications at these two sites could increase the stability of neuronal MTs (SONG
560 AND BRADY 2015). Interestingly, replacing the a.a. 35- 47 region of TBA-7 with the sequence
561 from MEC-12 that contains lysine 40 (the site for α-tubulin acetylation) did not affect the TBA-7
562 function (Figure 6D), suggesting that the absence of MT acetylation site in TBA-7 was not
563 responsible for its activity in preventing ectopic neurite growth.

564 Since TBA-7 lacks some modification sites (e.g. Q31 and E445) that could stabilize MTs,
565 our results suggest that TBA-7 may be a MT-destabilizing tubulin isotype, as compared to MEC-
566 12. In wild-type animals, TBA-7 incorporation into the 15-p MTs with MEC-7 and MEC-12 may
567 reduce MT stability; when TBA-7 is not available, more MEC-12 and possibly other α-tubulin
568 isotypes replace TBA-7 and this replacement alters MT dynamics to produces hyperstable MTs.

569 The *tba-7(u1015 lf); mec-7(u1017 neo)* double mutant had an ALM-PN that was similar
570 in length to that in *mec-7(u1017)* single mutants (Figure 6A), but the double mutant additionally

produced up to 4 and 5 short ectopic neurites sprouting from the ALM and PLM cell bodies, respectively; this phenotypes was rarely observed in *mec-7(u1017)* animals (Figure 6E and F). These results suggest that an additive effect occurs in the double mutant. Treating *tba-7(u1015)* and *mec-7(u1017)* single mutants with paclitaxel did not produce the double mutant phenotype, probably because the effect of paclitaxel on neurite growth is weak (KIRSZENBLAT *et al.* 2013).

Mutations in MT-associated Kinesins affect TRN neurite growth

Since motor proteins and MAPs regulate MT dynamics (AKHMANOVA AND STEINMETZ 2015), we expected mutations in MAP genes to cause similar phenotype to those of some of the tubulin mutations. Indeed, GHOSH-ROY *et al.* (2012) found and we have confirmed that the loss of the MT-depolymerizing kinesin *klp-7* induced the growth of an ectopic posterior neurite in ALM neurons (Figure 6B). KLP-7 belongs to the kinesin-13 family of catastrophe factors that bind to MT plus-ends and promotes depolymerization, thus generating dynamic microtubules (HAN *et al.* 2015). Importantly, as with the tubulin neomorphs, we found that the growth of the ectopic ALM-PN in *klp-7* mutants was suppressed by *mec-7* and *mec-12 lf* mutations but not enhanced by *mec-7 neo* mutations. These results suggest that the mutated MEC-7 proteins may render MTs hyperstable by reducing their interaction with KLP-7 or by making the MTs insensitive to the action of KLP-7.

Our screen yielded a mutation in a second kinesin gene, *klp-11*. The putative *klp-11* null allele *u1024* (Q53*) caused a moderate shortening of ALM-AN and PLM-AN without affecting PLM-PN; in the mutants, ALM-AN failed to extend beyond the metacorpus of the pharynx and PLM-AN did not reach the vulva (Figure S8). A *klp-11* deletion allele, *tm374*, gave the same phenotype. *klp-11* codes for a homolog of human KIF3B, a subunit of the plus end-directed kinesin-II motor complex. Although Kinesin-II motor mainly drives intraflagellar transport in the

cilia, studies have also shown that Kinesin-II can function in fast, anterograde axonal transport of vesicles in Drosophila (TAKEDA *et al.* 2000) and is required for axon growth and regeneration in mouse (GUMY *et al.* 2013). These data are consistent with KLP-11 being a positive regulator of neurite growth in TRNs. The selectivity of the *klp-11* effect on the ANs and not the PNs may relate to the polarity of the MTs they contain. MTs in the anterior neurites of TRNs have uniform polarity with all the plus ends oriented outward from the cell body, whereas the MTs in the PLM-PN have mixed polarity, containing both minus-end-out and plus-end-out MTs (CHALFIE AND THOMSON 1979; HSU *et al.* 2014). Thus, the use of minus end-directed motor proteins could support the growth of PLM-PN in the absence of KLP-11. Moreover, the moderate shortening of the ANs also suggests redundancy among the kinesin motor proteins. These results support the hypothesis that MTs promote TRN neurite growth by serving as tracks for the transport of membrane-bound vesicles.

The F-box containing protein MEC-15 is required for tubulin neomorphic phenotype

The putative *mec-15* null allele *u1008* (Q194*) was isolated from our main screen because the mutation caused the shortening of both PLM-AN and PLM-PN. Another null allele *u75* (Q118*) caused the same phenotype (Figure 7A). *mec-15* encodes a protein that contains a F-box at the N-terminus and four WD-40 repeats in the middle. Previous work from our lab found that *mec-15* is required for touch sensitivity and chemical synapse development in TRNs (BOUNOUTAS *et al.* 2009b). We found that the ALM-AN and PLM-AN in *mec-15* mutants could not fully extend the synaptic branch (Figure 7A), which may have caused the defects in synaptic development.

From the screen for suppressors of *mec-7(u278)* neomorph, we identified another *mec-15* null allele *u1024* (R27*), which strongly suppressed the growth of ectopic ALM-PN in *mec-*

617 *7(u278 neo)* animals. This suppression is cell-autonomous and depends on the F-box of MEC-15;
618 the expression of the wild-type MEC-15 from the TRN-specific *mec-18* promoter in *mec-15*(*lf*);
619 *mec-7(u278 neo)* double mutants restored the ectopic ALM-PN, but the expression of MEC-15
620 proteins that lacked or had a truncated the F-box domain could not (Figure 7C and D). Since F-
621 box is the substrate recognition subunit of the Skp, Cullin, F-box containing E3 ubiquitin ligase
622 complex (known as the SCF complex), our results suggest that ubiquitination is involved in
623 stabilizing the MTs in *mec-7(neo)* mutants. One hypothesis is that some unidentified MT-
624 destabilizing molecule is normally ubiquitinated and targeted for degradation in a MEC-15-
625 dependent manner. This unknown protein would be abnormally accumulated in TRNs to reduce
626 MT stability, which caused the shortening of the main neurites and their branches in *mec-15(lf)*
627 single mutants and the suppression of ALM-PN in *mec-15(lf)*; *mec-7(u278 neo)* double mutants;
628 the double mutants no longer have the hyperstable MTs. We also observed similar suppression of
629 the ectopic growth of ALM-PN in *mec-15(lf); mec-7(u1017 neo)*, *mec-15(lf); tba-7(lf)*, and *mec-*
630 *15(lf); klp-7(lf)* double mutants (Figure 7D), supporting the hypothesis that MEC-15-dependent
631 ubiquitination is needed for the increase of MT stability in the regulation of neurite growth.

632 **Tubulin mutations induce excessive neurite growth independent of MEC-17/α-TAT**

633 Our lab previously reported that the α-tubulin acetyl-transferase (α-TAT) MEC-17,
634 which acetylates MEC-12 in the MTs, is required for the formation of 15-p MTs, as well as MT
635 bundling and organization (TOPALIDOU *et al.* 2012). Although the loss of MEC-17 does not
636 significantly reduce MT acetylation due to the redundancy with its paralog ATAT-2, *mec-17* null
637 mutants showed defects in touch sensitivity, neurite growth and morphology, and vesicle
638 transport; these defects were rescued by expressing a catalytically inactive version of MEC-17,

639 indicating that non-enzymatic activity of MEC-17 is responsible for normal neurite formation
640 (TOPALIDOU *et al.* 2012; NEUMANN AND HILLIARD 2014).

641 Although the ALM neurons in *mec-17*(*lf)* mutants also grew an ectopic posterior neurite,
642 the Mec-17 phenotype is quite different from the phenotypes of the *mec-7* or *mec-12 neo* mutants
643 in the following ways. 1) the ALM-PN in *mec-17* animals grows beginning at the L4 stage,
644 whereas it was present as early as the L1 stage in *mec-7* and *mec-12 neo* mutants, and *tba-7* and
645 *klp-7 lf* mutants; 2) the ALM-PN in *mec-17* null mutants was longer at 25 °C than at 15 °C,
646 whereas the opposite was seen in tubulin neomorphs, which have a longer ALM-PN at 15 °C
647 than at 25 °C (Figure 8A); 3) excessive swelling and looping of the TRN neurites were observed
648 in *mec-17* mutants (TOPALIDOU *et al.* 2012) but not the other mutants; 4) *mec-17* mutants had
649 twice as many actively growing MTs as the wild-type animals, indicating increased dynamics
650 (NEUMANN AND HILLIARD 2014), whereas the other mutants presumably caused the formation of
651 hyperstable MTs. Interestingly, treatment with paclitaxel, which decreases MT dynamics,
652 partially suppressed the growth of ALM-PN in *mec-17(lf)* mutants but not in *mec-7* and *mec-12*
653 *neo* mutants or *tba-7* or *klp-7 lf* animals (Figure 8B). Moreover, when we combined the *mec-*
654 *17(ok2109 lf)* allele with the *mec-7(u1017 neo)* allele or *tba-7(u1015 lf)* allele, additive effects
655 were observed for the length of both ALM-PN and PLM-PN (Figure 8C). Together, our data
656 indicate that the loss of MEC-17 and the mutations in tubulin isotypes may induce excessive,
657 posteriorly directed neurite growth through different mechanisms.

658 One such difference in mechanism is the differential dependency on the guanine
659 nucleotide exchange factor TIAM-1, which promotes the growth of a posteriorly directed neurite
660 in the bipolar PLM neurons (ZHENG *et al.* 2016). *tiam-1* null mutations suppressed the growth of
661 ALM-PN in *mec-17(lf)* mutants but not in *mec-7* and *mec-12 neo* mutants and *tba-7(lf)* mutants

(Figure 8D). Because TIAM-1 promotes neurite extension through the Rac1 GTPase, which presumably regulates the dynamics of actin cytoskeleton (ZHENG *et al.* 2016), the loss of MEC-17 may activate TIAM-1 and induce actin remodeling, whereas the MT-stabilizing tubulin mutations do not evoke TIAM-1 to promote posterior outgrowth.

Discussion

Neuronal morphogenesis requires an optimal MT stability

MTs both support and regulate neurite growth. As the building block of MTs, α- and β-tubulins determine the structural properties of MTs and also mediate their interaction with motor proteins and MAPs. As a result, any alteration in the tubulin proteins can potentially lead to changes in MT dynamics, which then affects neurite formation, guidance, and extension. In this study, we analyzed the effects of 67 tubulin missense mutations on neurite development in *C. elegans* touch receptor neurons. Based on the phenotypes, we categorized these mutations into three classes: loss-of-function (*lf*), antimorphic (*anti*), and neomorphic (*neo*) mutations. 1) *lf* mutations cause only mild neurite growth defects by reducing MT stability moderately; 2) *anti* mutations block MT polymerization and cause severe neurite growth defects; 3) *neo* mutations cause excessive neurite growth by inducing hyperstable MTs (Figure 9). The directionality of the excessive neurite in ALM reflects its potential to grow towards the posterior. In fact, about 30% of the adult ALM neurons have a very short (less than one cell body length) posterior protrusion, and manipulation of cellular signaling (e.g. activating the small GTPase Rac or altering the recycling endosome pathway) can induce the production of ALM-PN (ZHENG *et al.* 2015b; ZHENG *et al.* 2016). Thus, the ectopic growth of ALM-PN may serve as an indication for altered cytoskeletal organization.

The correlation between the amount of neurite growth and the stability of MTs suggests that MT structure and dynamics are major determinants of neurite growth. Given the great number of proteins involved in both positively and negatively regulating MT assembly and disassembly (MIMORI-KIYOSUE 2011), our results support that an optimal level of MT stability is required for proper neuronal morphogenesis. This hypothesis is further supported by the finding that negative regulators of MT stability, such as the α-tubulin isotype TBA-7 and the MT-destabilizing kinesin-13 KLP-7, prevent excessive TRN neurite growth.

We suspect that other MT destabilizers are also important for TRN neurite development and that these destabilizing proteins are, in turn, regulated by the F-box containing protein MEC-15, perhaps by its involvement in ubiquitination and protein degradation. Loss of *mec-15* results in TRNs with shorter ANs and PNs. Since *mec-15(lf)* is epistatic with regard to neurite growth to the mec-7(*neo*), *mec-12(neo)*, *tba-7(lf)*, and *klp-7(lf)* mutations, MEC-15 is likely to reduce the amount of, as yet, unknown MT destabilizers.

Structure-function analysis of tubulin mutations

The large number of missense mutations analyzed in this study allowed us to perform structure-function analysis of neuronal tubulin proteins in living animals. Mapping the altered amino acid residues onto the *Bos taurus* tubulin α/β heterodimer structure 1JFF (NOGALES *et al.* 1998), we found that *lf* mutations mostly affect residues located in the interior of the structure and possibly disrupt protein folding. *anti* mutations affect residues that participate in GTP binding, intradimer interaction, or interdimer interactions. *neo* mutations mostly alter residues on the exterior surface and probably perturb the association of motor proteins and MAPs with MTs (Figure 4 and 9).

Although similar structure-function relationship studies were conducted before in yeast α-tubulin *TUB1* and β-tubulin *TUB2* and Drosophila testis-specific *β2*-tubulin (REIJO *et al.* 1994; FACKENTHAL *et al.* 1995; RICHARDS *et al.* 2000), our work provides another model to study the properties of tubulin proteins. In fact, our findings are consistent with those previous studies. For example, yeast *TUB1* mutations that caused supersensitivity to the MT-destabilizing drug benomyl mainly altered amino acids involved in GTP binding (e.g. D70) and intradimer (e.g. E98) and interdimer interaction; the change of equivalent residues in MEC-12 (D69 and E97) were identified in *mec-12 anti* mutants. Similarly, some Drosophila *β2*-tubulin mutations (S25L and G96E) that made MTs less stable (FACKENTHAL *et al.* 1995) affected the same or the adjacent residue in *mec-7* antimorphs [*u319* (S25F) and *u430* (A97V)]. On the other hand, yeast *TUB1* mutations that conferred benomyl-resistance mostly affect the residues exposed to the outer surface of the MTs (RICHARDS *et al.* 2000), and *mec-7 neo* mutations similarly led to increased resistance to colchicine. Therefore, comparative studies using the three different organisms can help identify key residues in the tubulin structure responsible for various MT functions.

Modeling the effects of neuronal tubulin mutations

We have used the *C. elegans* TRNs as a model to study neuronal MTs, which are much more stable and have different types of post-translational modification than the MTs in dividing cells (BAAS *et al.* 2016). Clinical studies in the past five years identified more than 100 missense mutations in tubulin genes that cause a wide spectrum of neurodevelopmental disorders, such as microcephaly, lissencephaly, polymicrogyria, and cortical malformation, along with severe defects in axon guidance and growth, including the complete or partial absence of corpus callosum, defects in commissural fiber tracts, and degeneration of motor and sensory axons

(TISCHFIELD *et al.* 2011; CHAKRABORTI *et al.* 2016). Patients carrying different tubulin mutations often display distinct symptoms, but the complexity of the human nervous system makes it difficult to analyze the impact of specific mutations at the cellular level.

Combining CRISPR/Cas9-mediated genome editing with *in vivo* examination of TRN morphology, we were able to create several disease-causing human β-tubulin mutations in the *C. elegans mec-7* gene and examined their effects on neurite growth at a single neuron resolution. Our phenotypic evaluation was largely consistent with previous characterization of those mutations, suggesting that the TRN system could be instrumental to model the effects of human tubulin mutations identified in the clinic.

In fact, many disease-causing tubulin mutations alter amino acids that are physically adjacent to or located in the same region as the ones affected in our mutants, suggesting that they may affect MT stability in similar ways. By mapping 51 TUBA1A, 24 TUBB2B, and 19 TUBB3B mutations that were clinically identified onto the tubulin structure, we could correlate the location of some of the affected residues with the resulting clinical manifestation (Table S4). For example, 7/8 (87.5%) mutations that alter residues involved in GTP binding caused complete agenesis of corpus callosum, an indication of severe defects in axonal growth, whereas only 5/23 (21.7%) changes of residues in the interior of the structure and 10/32 (31.2%) mutations of residues involved in MAP binding did so (Table S4).

However, position of the mutated residues alone could not determine the effects of the missense mutation; each specific mutation should be evaluated individually. For example, the B5-to-H5 loop of β-tubulin (from V170 to V179) is in contact with the GTP molecule and four strong *mec-7 anti* mutations (P171S, P171L, S176F, and V179A) were mapped to this loop. Unexpectedly, S172P mutation led to a *lf* phenotype and P173L mutation caused no defects in

753 TRNs. One possible explanation is that S172 and P173 are further away from the GTP binding
754 site and thus are less important than P171 and S176.

755 The identity of the residue replacing the wild type one also plays a critical role. For
756 instance, *u278* (C303Y) was the strongest *mec-7* neomorph, but *gk286001* (C303S) had no effect
757 at all; since both tyrosine and serine have the polar hydroxyl group, the bulky phenyl group of
758 the tyrosine may be responsible for disrupting some MT functions. Moreover, the *u1058* (A302T)
759 mutation also caused a strong *mec-7(neo)* phenotype. A302 and C303 on the H9-to-B8 loop are
760 exposed to the exterior of MTs but are not located on the major landing surface (H11 and H12)
761 for motor protein and MAPs. Our results suggest that A302 and C303 may represent a previously
762 unrecognized site of interaction between the MTs and their associated proteins. Even for residues
763 located on H11 and H12, the effects of their mutation can be different. *u1059* (R380S) is a *mec-7*
764 neomorph, whereas *u1060* (E410K) allele produced an antimorph-like phenotype, suggesting
765 that the impact of the missense mutation depends on how the interaction of MTs with the motor
766 proteins or MAP is affected by the amino acid change.

767 **MT-destabilizing tubulin isotype and "multi-tubulin hypothesis"**

768 The presence of multiple tubulin genes in eukaryotic genomes, their subtle differences in
769 the protein sequences, and their functional differences led to the "multi-tubulin hypothesis." In
770 multicellular organism, the tubulins may have distinct expression patterns, *e.g.* Drosophila *β2*-
771 tubulin is only expressed in the male germline (KEMPHUES *et al.* 1980); human TUBB3B is
772 highly enriched in the nervous system, whereas TUBB2B is expressed in many tissues
773 (SULLIVAN AND CLEVELAND 1986). In single-cell organisms like *Tetrahymena*, different β-
774 tubulin isotypes are spatially separated; some are only used to make the nuclear MTs of the
775 mitotic apparatus, and some are only detected in the MTs of somatic cilia and basal bodies

776 (PUCCIARELLI *et al.* 2012). Our studies, however, found that two distinct α-tubulin isotypes
777 (MEC-12 and TBA-7) could have different functions when both incorporated into the same MTs
778 in the same neurons; MEC-12 promotes stability and TBA-7 promotes instability.

779 The abundance of large diameter 15-p MTs in the TRNs requires MEC-12, but the role of
780 TBA-7 is to increase MT dynamics and to prevent the ectopic growth of posteriorly directed
781 neurites in ALMs. Thus, TBA-7 is a MT-destabilizing tubulin isotype, and this destabilizing
782 activity depends on the absence of potential polyamination and polyglutamination sites that
783 could increase MT stability. Our results are consistent with early *in vitro* experiments suggesting
784 that TUBB3 (also known as β_{III}) also promotes MT dynamics; removal of TUBB3 from the brain
785 extract resulted in a tubulin mixture that assembled much more rapidly than the unfractionated
786 control (BANERJEE *et al.* 1990), and MTs assembled from the purified $\alpha\beta_{III}$ heterodimers were
787 considerably more dynamic than MTs made from the $\alpha\beta_{II}$ and $\alpha\beta_{IV}$ dimers (PANDA *et al.* 1994).
788 However, the long-standing question is whether some tubulin isotypes do destabilize MTs *in vivo*.
789 Our findings suggest the answer is yes. A balanced incorporation of multiple tubulin isotypes
790 into the same MT structure is critical to generate MTs with the optimal stability.

791 The absence of post-translational modification sites in tubulin isotypes may lead to
792 functional diversity. In addition to TBA-7, among the other eight *C. elegans* α-tubulin isotypes,
793 TBA-8 and TBA-5 also lack the Q31 for polyamination, and TBA-6 lacks the E445 for
794 polyglutamination; all nine human α-tubulins have Q31, but TUBAL3 has a short C-terminal tail
795 and does not contain potential polyglutamination sites (Figure S9). The incorporation of those
796 tubulin isotypes may be a general regulatory mechanism to control MT stability.

797 Moreover, *mec-12* and *tba-7* do not appear to be redundant, because the *tba-7 lf* mutation
798 alone produced uncontrolled growth. Moreover, both *mec-12 lf* mutants and *mec-12; tba-7*

799 double *lf* mutants retained the ability to grow out a normal amount of neurites, suggesting strong
800 genetic redundancy among the α-tubulins with regards to supporting neurite growth.
801 Different contributions of tubulin isotypes to MT dynamics were also observed in *C.*
802 *elegans* embryogenesis (HONDA *et al.* 2017). The spindle MTs required two β-tubulins (TBB-1
803 and TBB-2), but TBB-2 was incorporated into the MTs twice as much as TBB-1; the loss of
804 TBB-2 caused a dramatic decrease in MT growth rate and an increase in catastrophe frequency,
805 leading to highly unstable MTs, whereas the loss of TBB-1 only slightly reduced growth rate.
806 These data support the "multi-tubulin concept" that different tubulin isotypes have distinct
807 functions in the same cells.
808
809
810 **Materials and Methods**
811 **Strains and genetic screens**
812 *C. elegans* wild type (N2) and mutant strains were maintained at 20 °C as previously
813 described (BRENNER 1974). Alleles listed in Table S1 and S2 were isolated by visually screening
814 for mutants with TRN differentiation defects using TU4069, which carries *uIs115 [mec-*
815 *17p::RFP]* for the visualization of the TRNs, as the starter strain and ethyl methanesulfonate as
816 the mutagen. Mutants were outcrossed with wild type, and the phenotype-causing mutations
817 were identified as previously described by whole-genome resequencing (ZHENG *et al.* 2013) or
818 by complementation tests with reference alleles. *mec-7* alleles *e1343*, *e1505*, *e1527*, *e1522*, *n434*,
819 *u10*, *u18*, *u22*, *u48*, *u58*, *u98*, *u127*, *u129*, *u162*, *u170*, *u223*, *u225*, *u278*, *u234*, *u249*, *u262*, *u275*,
820 *u283*, *u305*, *u319*, *u428*, *u429*, *u430*, *u433*, *u449*, and *u445*, and *mec-12* alleles *e1605*, *e1607*,
821 *u50*, *u63*, *u76*, and *u241* were previously isolated (CHALFIE AND SULSTON 1981; CHALFIE AND
822 AU 1989; SAVAGE *et al.* 1994) and re-examined in this study.

823 *u1056* to *u1060* alleles were created through CRISPR/Cas9-mediated homologous
824 recombination (DICKINSON *et al.* 2013). Guide RNAs were designed according to the target
825 sequence closest to the desired codon change (Figure 5A). Recombination templates were
826 created by cloning the *mec-7* coding region and 466 bp 3'UTR sequence into the SalI and
827 BamHI sites of pBlueScript II SK (+) vector and then introducing the desired missense mutation
828 (red in Figure 5A), along with synonymous mutations (blue in Figure 5A) that change the guide
829 RNA target sites, using the Q5 Site-Directed Mutagenesis Kit from New England Biolabs (NEB;
830 Ipswich, MA). pDD162 constructs expressing Cas9 and specific guide RNAs were injected
831 together with the corresponding recombination template and marker *myo-2p::RFP* into TU4069
832 animals. F1s expressing RFP in the muscle were singled out and genotyped to identify
833 heterozygotes with successful edits, and F2s carrying homozygous mutations were then isolated
834 and examined for TRN morphology.
835 The *gk* alleles of *mec-7* and *mec-12* listed in Table 1 were generated in the million
836 mutation project (THOMPSON *et al.* 2013) and obtained from the Caenorhabditis Genetics Center,
837 which is funded by NIH Office of Research Infrastructure Programs (P40 OD010440). *klp-*
838 *7(tm2143)*, *klp-11(tm374)*, and *mec-12(tm5083)* were generated by the National Bioresource
839 Project of Japan, and *mec-12(gm379)* was kindly provided by Dr. Chun-Liang Pan at the
840 National Taiwan University.
841 Additional *mec-12* null alleles (*u1026*, *u1027*, and *u1028*) were generated by
842 CRISPR/Cas9-mediated genome editing targeting 5'-GAAGTAATTTCGATTCACATCGG-3'
843 in exon 2 of *mec-12* as described above (DICKINSON *et al.* 2013). Frameshift-causing mutations
844 were identified by sequencing the *mec-12* locus (Figure S1).

A second screen was conducted using TU4879 [*mec-7 (u278); uIs115 (mec-17p::RFP)*] as the starter strain, and mutants with significantly shortened ALM-PN were isolated. *mec-7* [*u1040* (G98E)], *mec-12* [*u1041* (G246E)], and *mec-15* [*u1042* (R26*)] were obtained from this screen as suppressors of *mec-7[u278* (C303Y) *neo]* mutants.

Constructs and Transgenes

A *tba-7::GFP* reporter (TU#1632) was made by cloning a 1.2 kb *tba-7* promoter and the entire coding region from the genomic DNA to wild-type genomic DNA into the Gateway pDONR221 P4-P1r vector; the resulting entry vector, together with the pENTR-GFP, pENTR-*unc-54*-3'UTR, and destination vector pDEST-R4-R3 were used in the LR reaction to create the final expression vectors. *mec-17p::tba-7(+)* (TU#1629) was created by cloning a 1.9 kb *mec-17* promoter and the *tba-7* coding sequence into pDONR221 P4-P1r and pDONR221 vectors, respectively, and assembling these entry vectors with pENTR-*unc-54*-3'UTR and the destination vector. Details about the Gateway cloning method by Life Technologies can be found at www.invitrogen.com/site/us/en/home/Products-andServices/Applications/Cloning/Gateway-Cloning.html. *tba-7(+)* locus, including the 1.2 kb promoter, coding region, and a 911-bp 3'UTR, was cloned using SalI and NotI into pBlueScript II SK(+) vector; NEB Q5 site-directed mutagenesis kit was then used to generate constructs expressing the TBA-7 variants shown in Figure 6D.

To rescue the *mec-15* mutants, we amplified the *mec-15(+)* locus that includes a 3.2 kb promoter, coding region, and a 951 bp downstream region and injected the purified PCR product to perform the rescue experiments. We used previously described TU#891 *[mec-18p::mec-15(+)]* construct (BOUNOUTAS *et al.* 2009b) to perform cell-specific rescue and to generate constructs that express truncated MEC-15 proteins shown in Figure 7C.

868 Transgenes *uIs31[mec-17p::GFP]* III, *uIs115[mec-17p::RFP]* IV, and *uIs134[mec-*
869 *17p::RFP]* V were used to visualize TRN morphology (ZHENG *et al.* 2015a). *jsIs821[mec-*
870 *7p::GFP::RAB-3]* was used to assess synaptic vesicle localization (BOUNOUTAS *et al.* 2009b).

871 **Electron microscopy**

872 We re-analyzed previously collected cross-section images of ALM neurites from wild
873 type animals (N501, N631, N933, and N934 from the Hall lab collection) and from *mec-7*
874 neomorphic mutants *u170* and *u278* (SAVAGE *et al.* 1994). The wild type animals had been fixed
875 by either chemical immersion fixation without tannic acid (samples N501, N631; HALL 1995) or
876 by high-pressure freezing/freeze substitution (HPF/FS) including tannic acid (samples N933,
877 N934; TOPALIDOU *et al.* 2012). The *mec-7* neomorphic alleles had also been fixed by chemical
878 immersion, without tannic acid.

879 For this study, we fixed *mec-7 lf (ok2152)*, *mec-12 lf (tm5083)*, and *tba-7 lf (u1015)*
880 adults using an HPF/FS protocol that included a first fixation in 0.5% glutaraldehyde + 0.1%
881 tannic acid and a second fix in 2% osmium tetroxide + 0.1% uranyl acetate (UAc), both at -90 °C,
882 followed by staining in 1% UAc in acetone at 0 °C. We also fixed adults of *mec-12(anti)* mutants,
883 *u950*, *u76*, and *u1021*, using HPF/FS using a similar protocol, but without tannic acid. Eighty-
884 nanometer transverse sections were collected at multiple positions along the ALM anterior
885 neurite and post-stained with uranium acetate and lead citrate. A Philips CM10 electron
886 microscope with an attached Morada digital camera (Olympus) was used to acquire the images.

887 For each animal, we counted the number of MTs in the ALMs and measured the MT
888 diameter on sections collected from at least five different positions along the ALM-AN; data
889 from ALML and ALMR were combined. For each strain, we examined sections from at three
890 different animals. For wild-type animals, *tba-7 lf* mutants, and *mec-7* neomorphs, we used at

least ten sections to measure the distance between two closest MT centers and the proportion of MT-occupied area to the cross-sectional area of the neurite.

Phenotype Scoring and Statistical Analysis

We measured the length of TRN neurites in at least 30 fourth stage larvae or young adults grown at 20° C, except where otherwise stated. Relative length of posteriorly directed neurites was calculated by dividing the neurite length by the diameter of the cell body. Defects in TRN anterior neurite length were assessed by counting the percentage of cells whose neurites failed to reach the vulva (for PLM) or the posterior pharyngeal bulb (for ALM); at least 50 cells were examined for each strain.

Fluorescence intensity of the RFP expressed from the *uIs134* transgene in the ALM cell body was used to measure TRN protein levels; intensity was calculated after manual background subtraction using ImageJ as previously described (CHEN AND CHALFIE 2015). Synaptic vesicle localization was quantified by calculating the percentage of animals in each of the four phenotypical categories: 1) normal localization to the PLM synaptic branch; 2) reduced intensity of the synaptic marker at the synapses as partial defect; 3) complete loss of normal localization to the synapse as complete defect; 4) localization to the PLM-PN as mistargeting. At least 50 adult animals were examined.

Acetylated α-tubulin staining using antibody [6-11B-1] (abcam, Cambridge, MA) was performed and analyzed as previously described (TOPALIDOU *et al.* 2012). For colchicine treatment, animals were grown in standard NGM agar plates containing different concentrations (from 0.06 mM to 2 mM) of colchicine before phenotypic analysis as described before (BOUNOUTAS *et al.* 2009a). Similarly, 100 nM paclitaxel was added to the NGM agar plates, L1 animals were placed onto the plates, and young adults were examined for TRN morphology.

PyMOL (SCHRODINGER 2015) was used to view the structure of α/β tubulin dimer (1jff.pdb; NOGALES *et al.* 1998) and to label affected residues in *mec-7* and *mec-12* mutants,.

For statistical analysis, ANOVA and the post hoc Dunnett's test or Tukey-Kramer test were used to identify significant difference between the mutants and wild type animals in multiple comparisons. Student's *t* test was used to find significant difference between two samples in paired comparisons. Single and double asterisks indicated $p < 0.05$ and $p < 0.01$, respectively. The χ^2 test was used for the categorical data to find significant difference between different strains.

Acknowledgements

We thank Dan Dickinson, Chun-Liang Pan, and Andrew Chisholm for sharing reagents. This work was supported by NIH Grant GM30997 (to M.C.) and OD 010943 (to D.H.H.). Core facilities for electron microscopy were supported by NICHD P30 HD71593 for the RFK-IDDRC at Albert Einstein College of Medicine.

References

Akhmanova, A., and M. O. Steinmetz, 2015 Control of microtubule organization and dynamics: two ends in the limelight. Nat Rev Mol Cell Biol 16**:** 711-726.

Baas, P. W., A. N. Rao, A. J. Matamoros and L. Leo, 2016 Stability properties of neuronal microtubules. Cytoskeleton (Hoboken) 73**:** 442-460.

Bahi-Buisson, N., K. Poirier, F. Fourniol, Y. Saillour, S. Valence *et al.*, 2014 The wide spectrum of tubulinopathies: what are the key features for the diagnosis? Brain 137**:** 1676-1700.

Banerjee, A., M. C. Roach, P. Trcka and R. F. Luduena, 1990 Increased microtubule assembly in bovine brain tubulin lacking the type III isotype of beta-tubulin. J Biol Chem 265**:** 1794-1799.

Bercher, M., J. Wahl, B. E. Vogel, C. Lu, E. M. Hedgecock *et al.*, 2001 mua-3, a gene required for mechanical tissue integrity in Caenorhabditis elegans, encodes a novel transmembrane protein of epithelial attachment complexes. J Cell Biol 154**:** 415-426.

948 Bounoutas, A., J. Kratz, L. Emtage, C. Ma, K. C. Nguyen *et al.*, 2011 Microtubule depolymerization in
949 Caenorhabditis elegans touch receptor neurons reduces gene expression through a p38 MAPK
950 pathway. Proc Natl Acad Sci U S A 108**:** 3982-3987.
951 Bounoutas, A., R. O'Hagan and M. Chalfie, 2009a The multipurpose 15-protofilament microtubules in C.
952 elegans have specific roles in mechanosensation. Curr Biol 19**:** 1362-1367.
953 Bounoutas, A., Q. Zheng, M. L. Nonet and M. Chalfie, 2009b mec-15 encodes an F-box protein required
954 for touch receptor neuron mechanosensation, synapse formation and development. Genetics
955 183**:** 607-617, 601SI-604SI.
956 Brenner, S., 1974 The genetics of Caenorhabditis elegans. Genetics 77**:** 71-94.
957 Buck, K. B., and J. Q. Zheng, 2002 Growth cone turning induced by direct local modification of
958 microtubule dynamics. J Neurosci 22**:** 9358-9367.
959 Chakraborti, S., K. Natarajan, J. Curiel, C. Janke and J. Liu, 2016 The emerging role of the tubulin code:
960 From the tubulin molecule to neuronal function and disease. Cytoskeleton (Hoboken) 73**:** 521-
961 550.
962 Chalfie, M., and M. Au, 1989 Genetic control of differentiation of the Caenorhabditis elegans touch
963 receptor neurons. Science 243**:** 1027-1033.
964 Chalfie, M., and J. Sulston, 1981 Developmental genetics of the mechanosensory neurons of
965 Caenorhabditis elegans. Dev Biol 82**:** 358-370.
966 Chalfie, M., and J. N. Thomson, 1979 Organization of neuronal microtubules in the nematode
967 Caenorhabditis elegans. J Cell Biol 82**:** 278-289.
968 Chalfie, M., and J. N. Thomson, 1982 Structural and functional diversity in the neuronal microtubules of
969 Caenorhabditis elegans. J Cell Biol 93**:** 15-23.
970 Challacombe, J. F., D. M. Snow and P. C. Letourneau, 1996 Actin filament bundles are required for
971 microtubule reorientation during growth cone turning to avoid an inhibitory guidance cue. J Cell
972 Sci 109 (Pt 8)**:** 2031-2040.
973 Chen, X., and M. Chalfie, 2015 Regulation of mechanosensation in C. elegans through ubiquitination of
974 the MEC-4 mechanotransduction channel. J Neurosci 35**:** 2200-2212.
975 Cleveland, D. W., 1987 The multitubulin hypothesis revisited: what have we learned? J Cell Biol 104**:**
976 381-383.
977 Dent, E. W., S. L. Gupton and F. B. Gertler, 2011 The growth cone cytoskeleton in axon outgrowth and
978 guidance. Cold Spring Harb Perspect Biol 3.
979 Dickinson, D. J., J. D. Ward, D. J. Reiner and B. Goldstein, 2013 Engineering the Caenorhabditis elegans
980 genome using Cas9-triggered homologous recombination. Nat Methods 10**:** 1028-1034.
981 Du, H., and M. Chalfie, 2001 Genes regulating touch cell development in Caenorhabditis elegans.
982 Genetics 158**:** 197-207.
983 Edde, B., J. Rossier, J. P. Le Caer, E. Desbruyeres, F. Gros *et al.*, 1990 Posttranslational glutamylation of
984 alpha-tubulin. Science 247**:** 83-85.
985 Fackenthal, J. D., J. A. Hutchens, F. R. Turner and E. C. Raff, 1995 Structural analysis of mutations in the
986 Drosophila beta 2-tubulin isoform reveals regions in the beta-tubulin molecular required for
987 general and for tissue-specific microtubule functions. Genetics 139**:** 267-286.
988 Fulton, C., and F. A. Simpson, 1976 Selective synthesis and utilization of flagellar tubulin: the multi-
989 tubulin hypothesis., pp. 987-1005 in *Cell Motility*, edited by R. Goldman, T. Pollard and J.
990 Rosenbaum. Cold Spring Harbor Publications, New York.
991 Ghosh-Roy, A., A. Goncharov, Y. Jin and A. D. Chisholm, 2012 Kinesin-13 and tubulin posttranslational
992 modifications regulate microtubule growth in axon regeneration. Dev Cell 23**:** 716-728.
993 Gumy, L. F., D. J. Chew, E. Tortosa, E. A. Katrukha, L. C. Kapitein *et al.*, 2013 The kinesin-2 family member
994 KIF3C regulates microtubule dynamics and is required for axon growth and regeneration. J
995 Neurosci 33**:** 11329-11345.

Hall, D. H., 1995 Electron microscopy and three-dimensional image reconstruction. Methods Cell Biol 48: 395-436.

Hamelin, M., I. M. Scott, J. C. Way and J. G. Culotti, 1992 The mec-7 beta-tubulin gene of Caenorhabditis elegans is expressed primarily in the touch receptor neurons. EMBO J 11: 2885-2893.

Han, X., K. Adames, E. M. Sykes and M. Srayko, 2015 The KLP-7 Residue S546 Is a Putative Aurora Kinase Site Required for Microtubule Regulation at the Centrosome in C. elegans. PLoS One 10: e0132593.

Hedgecock, E. M., J. G. Culotti and D. H. Hall, 1990 The unc-5, unc-6, and unc-40 genes guide circumferential migrations of pioneer axons and mesodermal cells on the epidermis in C. elegans. Neuron 4: 61-85.

Hilliard, M. A., and C. I. Bargmann, 2006 Wnt signals and frizzled activity orient anterior-posterior axon outgrowth in C. elegans. Dev Cell 10: 379-390.

Honda, Y., K. Tsuchiya, E. Sumiyoshi, N. Haruta and A. Sugimoto, 2017 Tubulin isotype substitution revealed that isotype composition modulates microtubule dynamics in C. elegans embryos. J Cell Sci.

Hoyle, H. D., and E. C. Raff, 1990 Two Drosophila beta tubulin isoforms are not functionally equivalent. J Cell Biol 111: 1009-1026.

Hsu, J. M., C. H. Chen, Y. C. Chen, K. L. McDonald, M. Gurling *et al.*, 2014 Genetic analysis of a novel tubulin mutation that redirects synaptic vesicle targeting and causes neurite degeneration in C. elegans. PLoS Genet 10: e1004715.

Jaglin, X. H., K. Poirier, Y. Saillour, E. Buhler, G. Tian *et al.*, 2009 Mutations in the beta-tubulin gene TUBB2B result in asymmetrical polymicrogyria. Nat Genet 41: 746-752.

Kemphues, K. J., E. C. Raff, R. A. Raff and T. C. Kaufman, 1980 Mutation in a testis-specific beta-tubulin in Drosophila: analysis of its effects on meiosis and map location of the gene. Cell 21: 445-451.

Kirszenblat, L., B. Neumann, S. Coakley and M. A. Hilliard, 2013 A dominant mutation in mec-7/beta-tubulin affects axon development and regeneration in Caenorhabditis elegans neurons. Mol Biol Cell 24: 285-296.

Konishi, Y., and M. Setou, 2009 Tubulin tyrosination navigates the kinesin-1 motor domain to axons. Nat Neurosci 12: 559-567.

Leandro-Garcia, L. J., S. Leskela, I. Landa, C. Montero-Conde, E. Lopez-Jimenez *et al.*, 2010 Tumoral and tissue-specific expression of the major human beta-tubulin isotypes. Cytoskeleton (Hoboken) 67: 214-223.

Liao, G., and G. G. Gundersen, 1998 Kinesin is a candidate for cross-bridging microtubules and intermediate filaments. Selective binding of kinesin to detyrosinated tubulin and vimentin. J Biol Chem 273: 9797-9803.

Liu, G., and T. Dwyer, 2014 Microtubule dynamics in axon guidance. Neurosci Bull 30: 569-583.

Lockhead, D., E. M. Schwarz, R. O'Hagan, S. Bellotti, M. Krieg *et al.*, 2016 The tubulin repertoire of C. elegans sensory neurons and its context-dependent role in process outgrowth. Mol Biol Cell.

Mapes, J., J. T. Chen, J. S. Yu and D. Xue, 2010 Somatic sex determination in Caenorhabditis elegans is modulated by SUP-26 repression of tra-2 translation. Proc Natl Acad Sci U S A 107: 18022-18027.

McKean, P. G., S. Vaughan and K. Gull, 2001 The extended tubulin superfamily. J Cell Sci 114: 2723-2733.

Mimori-Kiyosue, Y., 2011 Shaping microtubules into diverse patterns: molecular connections for setting up both ends. Cytoskeleton (Hoboken) 68: 603-618.

Mitani, S., H. Du, D. H. Hall, M. Driscoll and M. Chalfie, 1993 Combinatorial control of touch receptor neuron expression in Caenorhabditis elegans. Development 119: 773-783.

Mitchison, T., and M. Kirschner, 1984 Dynamic instability of microtubule growth. Nature 312: 237-242.

Neumann, B., and M. A. Hilliard, 2014 Loss of MEC-17 leads to microtubule instability and axonal degeneration. Cell Rep 6: 93-103.

1044 Nogales, E., S. G. Wolf and K. H. Downing, 1998 Structure of the alpha beta tubulin dimer by electron
1045 crystallography. Nature 391**:** 199-203.
1046 Panda, D., H. P. Miller, A. Banerjee, R. F. Luduena and L. Wilson, 1994 Microtubule dynamics in vitro are
1047 regulated by the tubulin isotype composition. Proc Natl Acad Sci U S A 91**:** 11358-11362.
1048 Papsdorf, K., J. Sacherl and K. Richter, 2014 The balanced regulation of Hsc70 by DNJ-13 and UNC-23 is
1049 required for muscle functionality. J Biol Chem 289**:** 25250-25261.
1050 Poirier, K., Y. Saillour, N. Bahi-Buisson, X. H. Jaglin, C. Fallet-Bianco *et al.*, 2010 Mutations in the neuronal
1051 ss-tubulin subunit TUBB3 result in malformation of cortical development and neuronal
1052 migration defects. Hum Mol Genet 19**:** 4462-4473.
1053 Prokop, A., 2013 The intricate relationship between microtubules and their associated motor proteins
1054 during axon growth and maintenance. Neural Dev 8**:** 17.
1055 Pucciarelli, S., P. Ballarini, D. Sparvoli, S. Barchetta, T. Yu *et al.*, 2012 Distinct functional roles of beta-
1056 tubulin isotypes in microtubule arrays of Tetrahymena thermophila, a model single-celled
1057 organism. PLoS One 7**:** e39694.
1058 Purro, S. A., L. Ciani, M. Hoyos-Flight, E. Stamatakou, E. Siomou *et al.*, 2008 Wnt regulates axon behavior
1059 through changes in microtubule growth directionality: a new role for adenomatous polyposis
1060 coli. J Neurosci 28**:** 8644-8654.
1061 Qu, C., T. Dwyer, Q. Shao, T. Yang, H. Huang *et al.*, 2013 Direct binding of TUBB3 with DCC couples
1062 netrin-1 signaling to intracellular microtubule dynamics in axon outgrowth and guidance. J Cell
1063 Sci 126**:** 3070-3081.
1064 Reijo, R. A., E. M. Cooper, G. J. Beagle and T. C. Huffaker, 1994 Systematic mutational analysis of the
1065 yeast beta-tubulin gene. Mol Biol Cell 5**:** 29-43.
1066 Richards, K. L., K. R. Anders, E. Nogales, K. Schwartz, K. H. Downing *et al.*, 2000 Structure-function
1067 relationships in yeast tubulins. Mol Biol Cell 11**:** 1887-1903.
1068 Sainath, R., and G. Gallo, 2015 Cytoskeletal and signaling mechanisms of neurite formation. Cell Tissue
1069 Res 359**:** 267-278.
1070 Savage, C., Y. Xue, S. Mitani, D. Hall, R. Zakhary *et al.*, 1994 Mutations in the Caenorhabditis elegans
1071 beta-tubulin gene mec-7: effects on microtubule assembly and stability and on tubulin
1072 autoregulation. J Cell Sci 107 (Pt 8)**:** 2165-2175.
1073 Schaefer, A. W., V. T. Schoonderwoert, L. Ji, N. Mederios, G. Danuser *et al.*, 2008 Coordination of actin
1074 filament and microtubule dynamics during neurite outgrowth. Dev Cell 15**:** 146-162.
1075 Schrodinger, LLC, 2015 The PyMOL Molecular Graphics System, Version 1.8, pp.
1076 Sirajuddin, M., L. M. Rice and R. D. Vale, 2014 Regulation of microtubule motors by tubulin isotypes and
1077 post-translational modifications. Nat Cell Biol 16**:** 335-344.
1078 Song, Y., and S. T. Brady, 2015 Post-translational modifications of tubulin: pathways to functional
1079 diversity of microtubules. Trends Cell Biol 25**:** 125-136.
1080 Song, Y., L. L. Kirkpatrick, A. B. Schilling, D. L. Helseth, N. Chabot *et al.*, 2013 Transglutaminase and
1081 polyamination of tubulin: posttranslational modification for stabilizing axonal microtubules.
1082 Neuron 78**:** 109-123.
1083 Sullivan, K. F., 1988 Structure and utilization of tubulin isotypes. Annu Rev Cell Biol 4**:** 687-716.
1084 Sullivan, K. F., and D. W. Cleveland, 1986 Identification of conserved isotype-defining variable region
1085 sequences for four vertebrate beta tubulin polypeptide classes. Proc Natl Acad Sci U S A 83**:**
1086 4327-4331.
1087 Takeda, S., H. Yamazaki, D. H. Seog, Y. Kanai, S. Terada *et al.*, 2000 Kinesin superfamily protein 3 (KIF3)
1088 motor transports fodrin-associating vesicles important for neurite building. J Cell Biol 148**:** 1255-
1089 1265.
1090 Tanaka, E., T. Ho and M. W. Kirschner, 1995 The role of microtubule dynamics in growth cone motility
1091 and axonal growth. J Cell Biol 128**:** 139-155.

Thompson, O., M. Edgley, P. Strasbourger, S. Flibotte, B. Ewing *et al.*, 2013 The million mutation project: a new approach to genetics in Caenorhabditis elegans. Genome Res 23**:** 1749-1762.

Tian, G., X. H. Jaglin, D. A. Keays, F. Francis, J. Chelly *et al.*, 2010 Disease-associated mutations in TUBA1A result in a spectrum of defects in the tubulin folding and heterodimer assembly pathway. Hum Mol Genet 19**:** 3599-3613.

Tischfield, M. A., H. N. Baris, C. Wu, G. Rudolph, L. Van Maldergem *et al.*, 2010 Human TUBB3 mutations perturb microtubule dynamics, kinesin interactions, and axon guidance. Cell 140**:** 74-87.

Tischfield, M. A., G. Y. Cederquist, M. L. Gupta, Jr. and E. C. Engle, 2011 Phenotypic spectrum of the tubulin-related disorders and functional implications of disease-causing mutations. Curr Opin Genet Dev 21**:** 286-294.

Topalidou, I., C. Keller, N. Kalebic, K. C. Nguyen, H. Somhegyi *et al.*, 2012 Genetically separable functions of the MEC-17 tubulin acetyltransferase affect microtubule organization. Curr Biol 22**:** 1057-1065.

Verhey, K. J., and J. Gaertig, 2007 The tubulin code. Cell Cycle 6**:** 2152-2160.

Yu, I., C. P. Garnham and A. Roll-Mecak, 2015 Writing and Reading the Tubulin Code. J Biol Chem 290**:** 17163-17172.

Zheng, C., M. Diaz-Cuadros and M. Chalfie, 2015a Dishevelled attenuates the repelling activity of Wnt signaling during neurite outgrowth in Caenorhabditis elegans. Proc Natl Acad Sci U S A 112**:** 13243-13248.

Zheng, C., M. Diaz-Cuadros and M. Chalfie, 2015b Hox Genes Promote Neuronal Subtype Diversification through Posterior Induction in Caenorhabditis elegans. Neuron 88**:** 514-527.

Zheng, C., M. Diaz-Cuadros and M. Chalfie, 2016 GEFs and Rac GTPases control directional specificity of neurite extension along the anterior-posterior axis. Proc Natl Acad Sci U S A 113**:** 6973-6978.

Zheng, C., S. Karimzadegan, V. Chiang and M. Chalfie, 2013 Histone methylation restrains the expression of subtype-specific genes during terminal neuronal differentiation in Caenorhabditis elegans. PLoS Genet 9**:** e1004017.

Gene	Allele	Mutation	Structural function	Classification	Morphological defects	Touch sensitivity	Expression
mec-7	*u319*	S25F	Tubulin folding	weak antimorph	moderately shortened neurites	-	semidominant
	u305, u1020	G34S	Lumen-facing loop	lf	short PLM-PN	±	recessive
	gk906464	G38E	Lumen-facing loop	N/A	no defects	+	N/A
	u58, u223	P61L	Lateral interaction	weak antimorph	moderately shortened neurites	−	semidominant
	u249	P61S	Lateral interaction	weak antimorph	moderately shortened neurites	−	semidominant
	gk337318	V64I	Tubulin folding	N/A	no defects	+	N/A
	u430	A97V	GTP binding	antimorph	short TRN neurites	−	recessive
	u222	G109E	Lateral interaction	weak antimorph	moderately shortened neurites	−	semidominant
	u429, u433	G141E	Tubulin folding	lf	short PLM-PN	−	recessive
	gk595364	G141R	Tubulin folding	lf	short PLM-PN	−	recessive
	u275	G148R	Tubulin folding	lf	short PLM-PN	−	recessive
	gk895768	T149I	Tubulin folding	neomorph	ectopic ALM-PN	±	recessive
	gk286003	R162Q	MAP binding	neomorph	ectopic ALM-PN	±	recessive
	u911	P171S	GTP binding	antimorph	short TRN neurites	−	dominant
	u957, u127, e1343	P171L	GTP binding	antimorph	short TRN neurites	−	semidominant
	u1056	S172P*	GTP binding	lf	short PLM-PN	−	recessive
	u1057	P173L*	GTP binding	N/A	no defects	+	N/A
	u48	S176F	GTP binding	antimorph	short TRN neurites	−	semidominant
	u449	V179A	GTP binding	antimorph	short TRN neurites	−	semidominant
	u10	S188F	Tubulin folding	lf	short PLM-PN	±	recessive
	u225	T214P	Tubulin folding	lf	short PLM-PN	±	recessive
	ky852	P220S	Tubulin folding	neomorph	ectopic ALM-PN	−	semidominant
	u262	N226Y	GTP binding	antimorph	short TRN neurites	−	semidominant
	gk286002	P243S	Intradimer interaction	lf	short PLM-PN	±	recessive
	u283	P243L	Intradimer interaction	antimorph	short TRN neurites	−	dominant
	u129, u958	G244S	Intradimer interaction	antimorph	short TRN neurites	−	dominant
	n434	N247I	Intradimer interaction	antimorph	short TRN neurites	−	dominant
	u162	D249N	Intradimer interaction	antimorph	short TRN neurites	−	dominant
	e1505	G269D	Tubulin folding	lf	short PLM-PN	±	recessive
	e1527	V286D	Lateral interaction	antimorph	short TRN neurites	−	dominant
	u445	M300V	Tubulin folding	antimorph	short TRN neurites	−	semidominant
	u98	M300T	Tubulin folding	antimorph	short TRN neurites	−	semidominant
	u1058	A302T*	MAP binding	neomorph	ectopic ALM-PN	±	semidominant
	u278	C303Y	MAP binding	neomorph	ectopic ALM-PN	−	semidominant
	gk286001	C303S	MAP binding	N/A	no defects	+	N/A
	gk286000	A314V	Tubulin folding	antimorph	short TRN neurites	−	semidominant
	e1522	F317I	Tubulin folding	lf	short PLM-PN	±	recessive
	u234	R318Q	Tubulin folding	lf	short PLM-PN	±	recessive
	u955	A352T	Intradimer interaction	antimorph	short TRN neurites	−	dominant
	u910, gk373602	P357L	Tubulin folding	antimorph	short TRN neurites	−	dominant

	u956	P358L	Tubulin folding	antimorph	short TRN neurites	−	dominant
	u428	G369E	Tubulin folding	lf	short PLM-PN	−	recessive
	u1017	L377F	MAP binding	neomorph	the growth of ectopic ALM-PN	±	recessive
	u1059	R380S*	MAP binding	neomorph	the growth of ectopic ALM-PN	±	recessive
	u18	A393T	Longitudinal interaction	antimorph	short TRN neurites	−	dominant
	gk285997	A393V	Longitudinal interaction	antimorph	short TRN neurites	−	dominant
	u170	E407L	MAP binding	neomorph	the growth of ectopic ALM-PN	±	recessive
	u1060	E410K*	MAP binding	antimorph	shortened TRN-ANs	−	semidominant
mec-12	*gk170196*	P32S	Lumen-facing loop	neomorph	the growth of ectopic ALM-PN	±	recessive
	gk170195	S50N	Lumen-facing loop	N/A	no defects	+	N/A
	gk636747	R60H	Lumen-facing loop	N/A	no defects	+	N/A
	u76	D69N	GTP binding	antimorph	short PLM-PN	−	recessive
	u1016	E97K	Intradimer interaction	antimorph	short PLM-PN	−	recessive
	u950, gk672907	S140F	GTP binding	antimorph	short PLM-PN	−	recessive
	gk600523	G142E	GTP binding	lf	no defects	±	recessive
	u1021, e1607	G144S	GTP binding	antimorph	short PLM-PN	−	recessive
	gk583647	L152F	Tubulin folding	N/A	no defects	+	N/A
	u50, e1605	H192Y	MAP binding	partial lf	no defects	−	recessive
	gk915672	E196K	MAP binding	neomorph	the growth of ectopic ALM-PN	±	recessive
	u1041	G246E	Tubulin folding	lf	no defects	±	recessive
	u917	V260I	MAP binding	neomorph	the growth of ectopic ALM-PN	±	recessive
	gk854211	P307L	MAP binding	N/A	no defects	+	N/A
	gk515972	V323I	Longitudinal interaction	neomorph	the growth of ectopic ALM-PN	±	recessive
	u241, u1019	G354E	Longitudinal interaction	antimorph	short PLM-PN	−	recessive
	gk341552	G365E	Lumen-facing loop	N/A	no defects	+	N/A
	u63	E415K	MAP binding	partial lf	no defects	±	recessive
	gm379	G416E	MAP binding	partial lf	no defects	±	recessive

Table Legends

Table 1. The *mec-7* and *mec-12* mutations analyzed in this study. Several mutations are represented by multiple alleles, whose phenotypes were found to be similar. For touch sensitivity, + indicate the average response to 5 anterior stimuli is above 4; ± indicate the average is between 4 and 1; − indicate the average is below 1. Partial *lf* alleles of *mec-12* showed some but not all of the *lf* phenotypes (see the text). Asterisks indicate that the mutation was originally found in humans and was created in *mec-7* gene through CRISPR/Cas9-mediated genome editing. Mapping of the amino acid residues to the structural domains was done according to Tischfield *et al.* (2011).

A

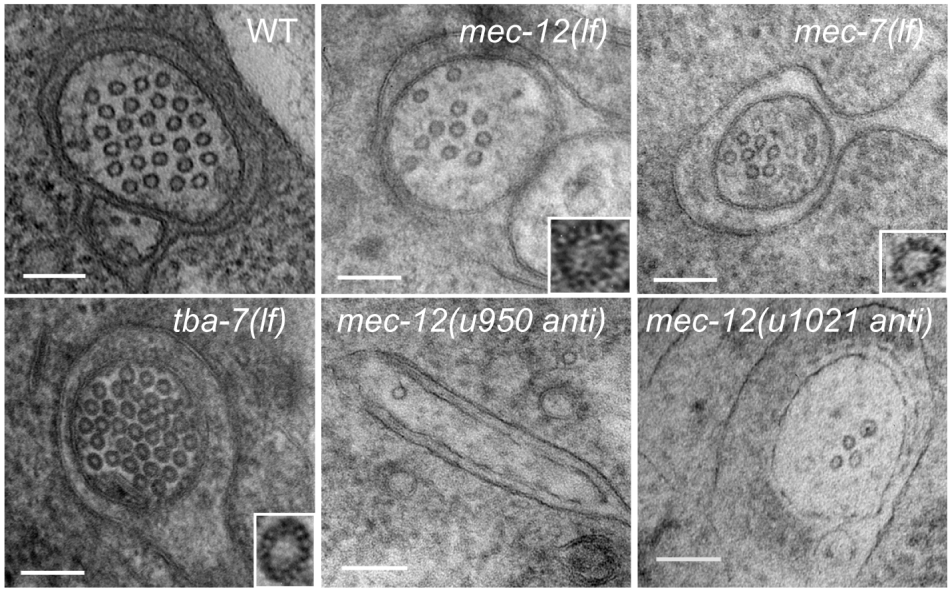

B

Genotype	Number of MTs	MT diameters (nm)	Center-center distance (nm)	MT-occupied area (%)
wild type	31.1 ± 7.3 (79)	21.5 ± 1.6 (126)	34.4 ± 1.0 (320)	46.7 ± 5.5 (38)
mec-7(ok2152 lf)	6.0 ± 2.2 (52)**	16.6 ± 1.4 (123)**		
mec-12(tm5083 lf)	7.4 ± 2.4 (36)**	21.3 ± 2.0 (103)		
tba-7(u1015 lf)	27.0 ± 10.1 (109)	22.4 ± 1.8 (248)**	32.3 ± 2.1 (278)**	57.2 ± 10.1 (74)**
mec-7(u170 neo)	18.0 ± 5.8 (25)**	22.7 ± 2.2 (192)**	31.7 ± 2.3 (148)**	58.6 ± 5.2 (20)**
mec-7(u278 neo)	20.6 ± 6.8 (23)**	22.5 ± 1.9 (176)**	32.9 ± 1.5 (164)**	59.0 ± 8.1 (18)**
mec-12(u76 anti)	1.6 ± 1.5 (52)**	17.6 ± 2.6 (53)**		
mec-12(u950 anti)	2.5 ± 2.1 (40)**	18.0 ± 2.0 (75)**		
mec-12(u1021 anti)	2.7 ± 2.4 (72)**	17.9 ± 1.8 (114)**		

Figure 1. MT structures in tubulin mutants. (A) Cross sectional images of ALM-AN in wild type and, *mec-12(tm5083 lf)*, *mec-7(ok2152 lf)*, *tba-7(u1015 lf) mec-12[u950* (S140F) *anti]* and *mec-12[u1021* (G144S) *anti]* mutants. MT structures in *mec-7(anti)* mutants were analyzed by Chalfie and Thomson (1982). Insets in the lower right corner of *mec-12(lf)*, *mec-7(lf)*, and *tba-7(lf)* animals show the protofilament structure of tannic acid stained MTs (4-fold enlarged). Scale bar = 100 nm. (B) Measures of MT structure and organization. Numbers of observations are shown in parentheses, and a Dunnett's test was performed to compare the mutants with the wild type. Throughout the figures, one asterisk represents a statistical significance of $p < 0.05$ and two asterisks indicate $p < 0.01$. [Note: Our earlier studies found that wild-type TRN MTs had much larger diameters than we find here (29.6 ± 0.4 nm; Chalfie and Thomson 1979). We could not explain the discrepancy between these and our current results. We are, nonetheless, very confident in the current calibration.]

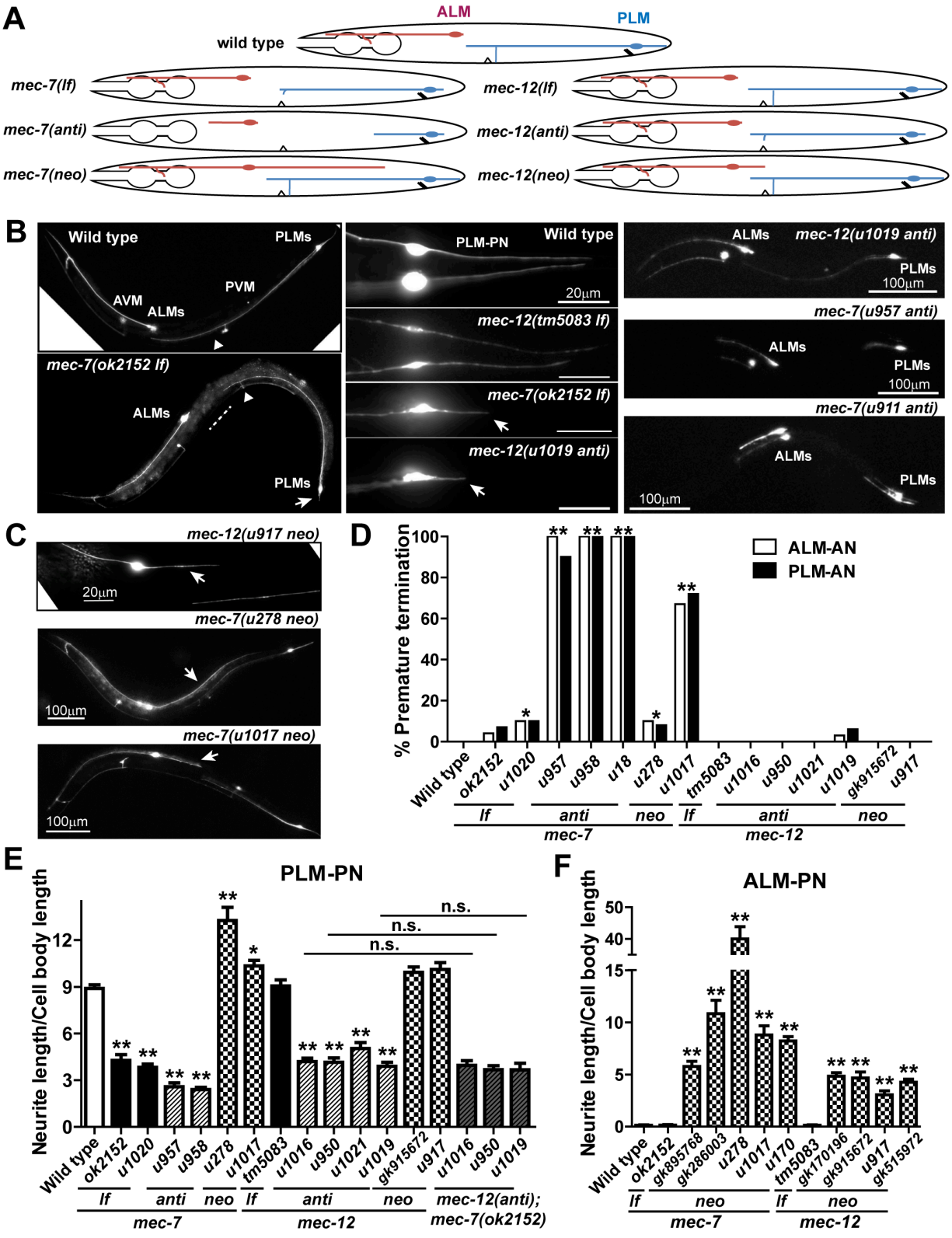

Figure 2. *mec-7* and *mec-12* mutations affect TRN neurite length. (A) Schematic diagram of ALM and PLM morphology in *mec-7* and *mec-12 lf*, *anti*, and *neo* mutants. (B) On the left panel, compared to the

wild-type animals, *mec-7(ok2152 lf)* animals showed an increased gap between PLM-AN and ALM cell body (dashed line) and significantly shortened PLM-PN (arrows). PLM-AN still extends beyond the position of the vulva indicated by the triangle. The middle panel showed PLM posterior neurites in the various animals. Arrows pointed to the shortened PLM-PN. The right panel displayed the TRN morphologies in *mec-12[u1019* (G354E) *anti]*, *mec-7[u957* (P171L) *anti]*, and *mec-7[u958* (G244S) *anti]* animals. (C) TRN morphology of *mec-12[u917* (V260I) *neo]*, *mec-7[u278* (C303Y) *neo]*, and *mec-7[u1017* (C377F) *neo]* animals. Arrows point to the ectopic ALM-PN. (D) The percentage of ALM and PLM cells that had significantly shortened anterior neurites (ALM-AN not reaching the posterior pharyngeal bulb and PLM-AN not extending beyond the vulva). Amino acid changes in the alleles can be found in Table 1. A χ^2 test for categorical data was used to compare mutants with the wild type. (E-F) The relative length of PLM-PN or ALM-PN in *mec-7* and *mec-12 lf*, *anti*, and *neo* mutant animals, as well as the double mutants of *mec-7(ok2151 lf)* with *mec-12 neo* alleles. Dunnett's test was used to analyze the data.

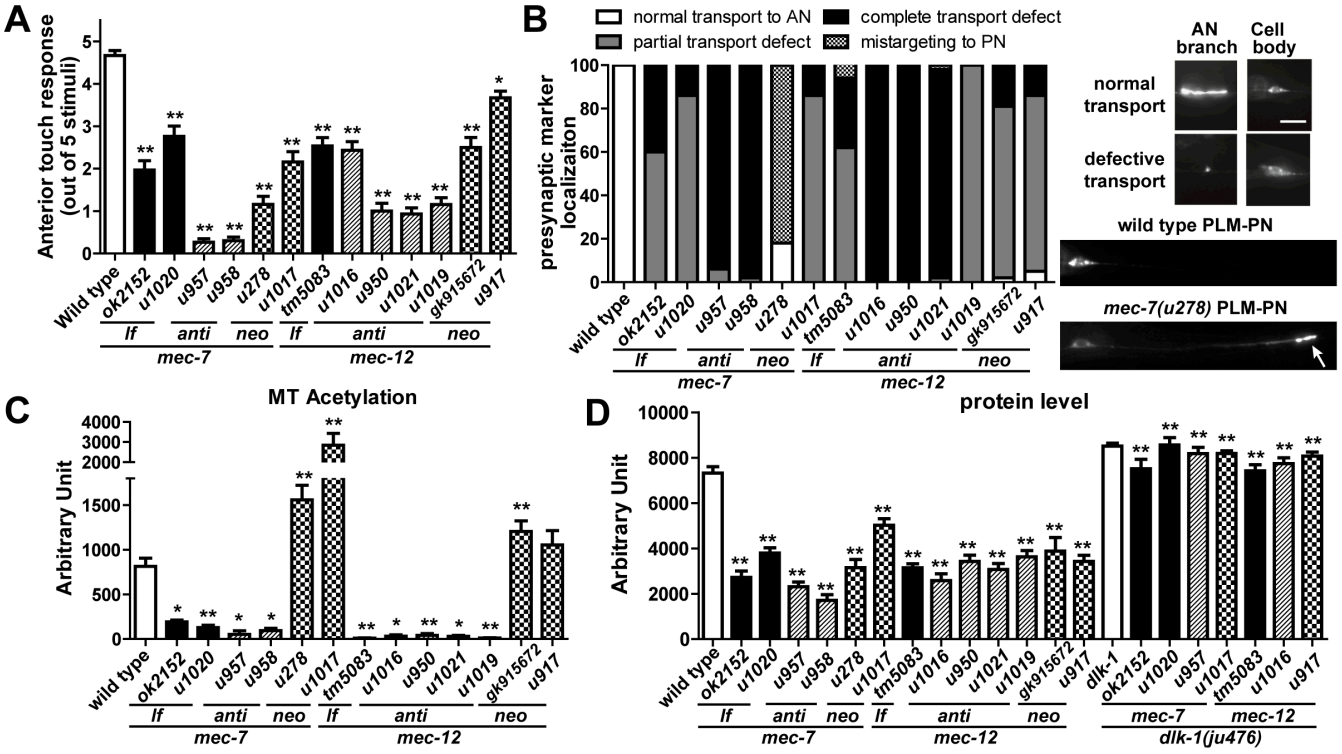

Figure 3. Effects of *mec-7* and *mec-12* mutations on TRN development and functions. (A) The average number of anterior touch responses of *mec-7* and *mec-12 lf*, *anti*, and *neo* mutants at the anterior side. (B) Defective targeting of the synaptic vesicle marker RAB-3::GFP in *mec-7* and *mec-12* mutant PLM neurons. RAB-3::GFP signal is found in patches where PLM-AN branches synapse onto target neurons in the wild-type ventral nerve cord. This targeting was partially or completely lost in many of the mutants; this loss in *mec-7(lf)* and *mec-12(anti)* mutants could be partly caused by the lack of PLM synaptic branch. In *mec-7(u278*; C303Y*)* mutants, however, the marker was mistargeted to the distal end of PLM-PN (arrow). (C) Immunofluorescent intensity of antibody labeling of acetylated α-tubulin. (D) Fluorescent intensity of the TRN marker *uIs134 [mec-17p::RFP]* in various *mec-7* and *mec-12* mutants and their doubles with *dlk-1 lf (ju476)* allele. Dunnett's tests were performed to compare the mutants with the wild type animals, and *t* tests with Bonferroni correction were used to identify significant difference between the tubulin single mutants and *dlk-1; mec-7* or *dlk-1; mec-12* double mutants.

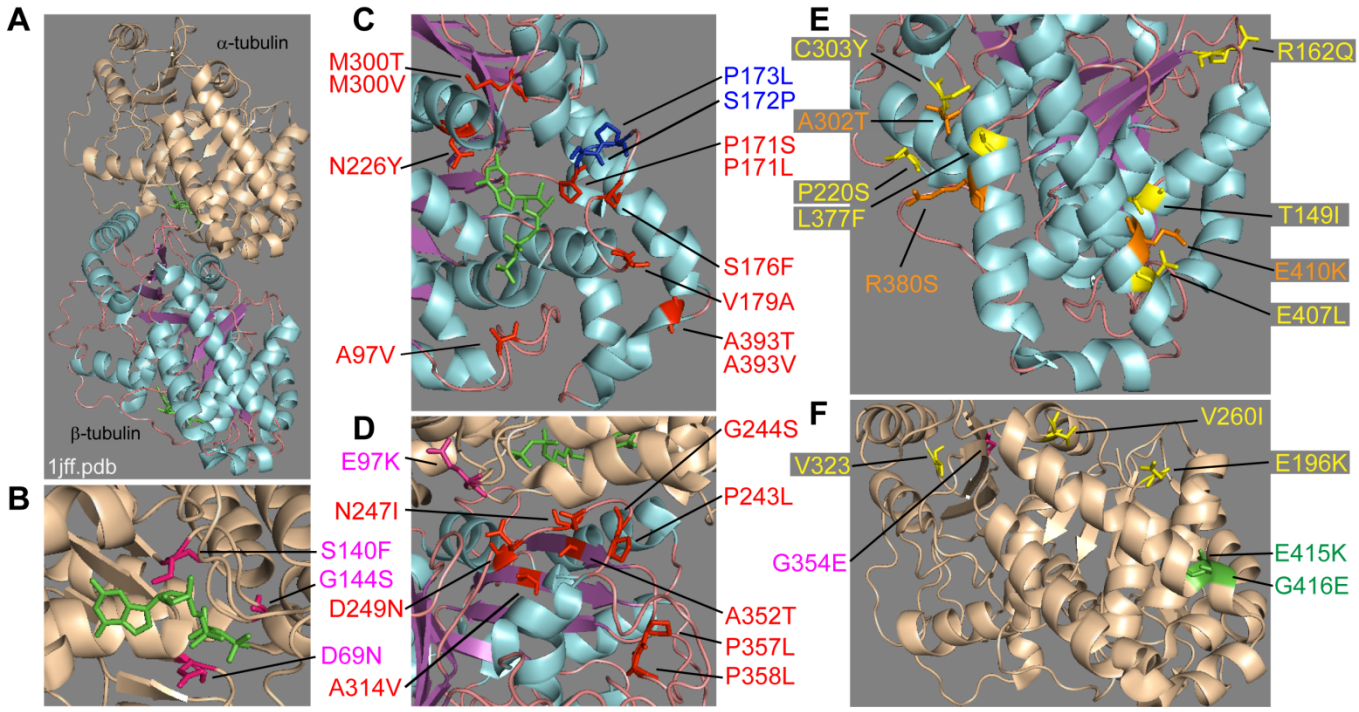

Figure 4. Position of amino acid residues changed in *mec-7* and *mec-12* mutants. (A) The structure of the α/β tubulin dimer (1jff.pdb) visualized using PyMOL. α-tubulin is in wheat, and β-tubulin is in cyan, magenta, and pink, which labels α-helices, β-sheets, and loops, respectively. GTP is labeled in green. (B-C) Amino acid changes around the GTP binding pocket in *mec-7* (red) and *mec-12* (pink) antimorphs. P173L and S172P (blue) are disease-associated mutations found in human TUBB3 that were engineered in *mec-7* to test their effects. (D) *mec-7* (red) and *mec-12* (pink) *anti* mutations mapped to intradimer interface. (E-F) Amino acid alterations in *mec-7* (E, yellow) and *mec-12* (F, yellow) *neo* alleles. A302T, R380S, and E410K (orange) were clinically identified TUBB3 mutations. E415 and G416 (green), mutated in *mec-12* partial *lf* alleles, are located at the exterior surface of α-tubulin.

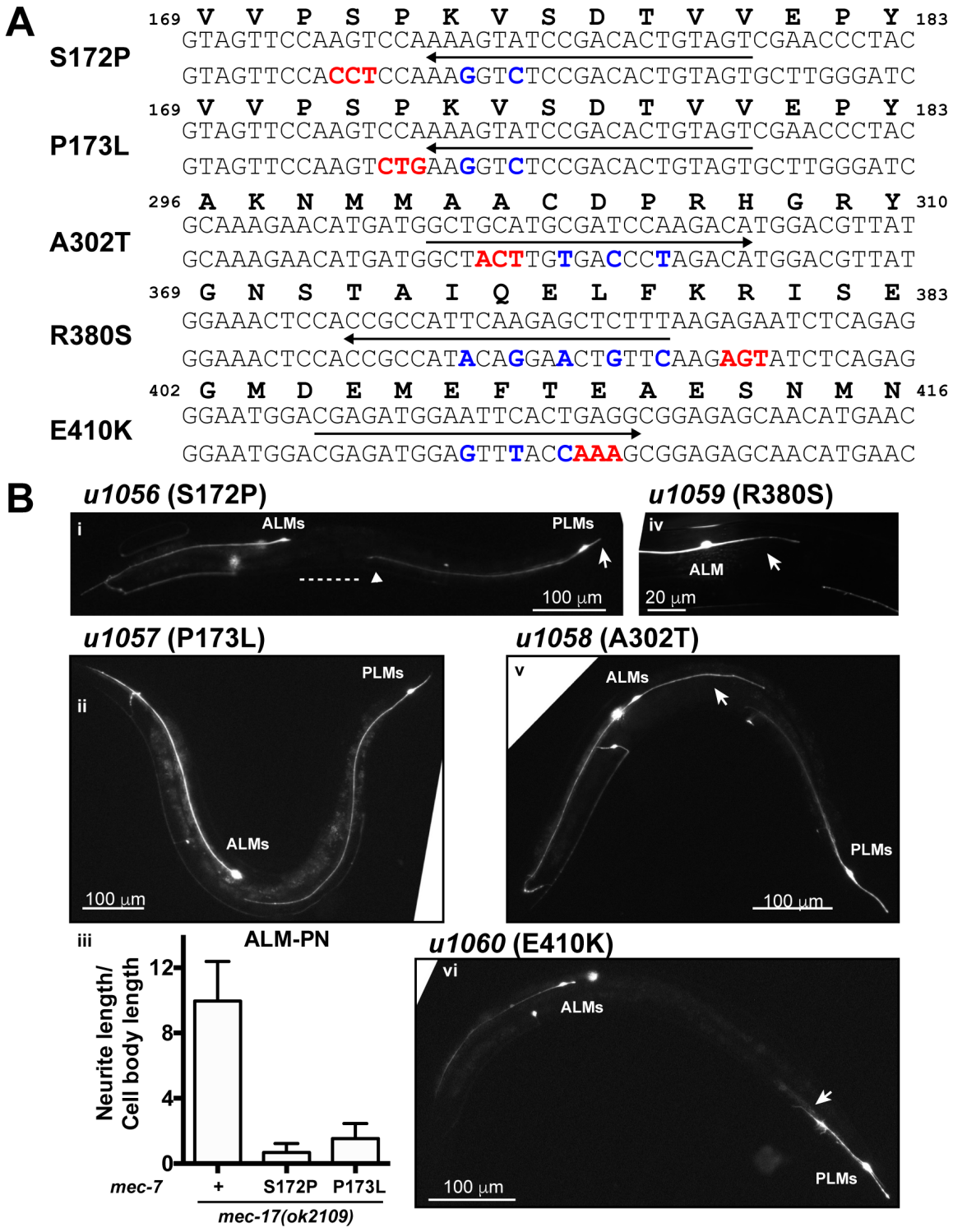

Figure 5. Modeling human tubulin mutations in *C. elegans* TRNs. (A) Sequence changes designed to introduce TUBB3 missense mutations in *mec-7* gene. For each mutation, the line with an arrow underscores the 20 bp DNA sequence for the guide RNA target, and the directionality of the arrow

indicates the strand of the target. The bottom DNA sequence contains the desired nonsynonymous (red) and synonymous mutations (blue) on the homologous repair template. Amino acids sequence with the positional information was shown on the top. (B) TRN morphologies of animals carrying the engineered missense mutations. For *u1056I* (i), dashed line, triangle, and the arrow indicate the gap from PLM-AN to ALM cell body, the position of the vulva, and the shortened PLM-PN, respectively. (iii) shows the length of ALM-PN in *mec-17; mec-7(u1056)* and *mec-17; mec-7(u1057)* double mutants. For *u1058* (v) and *u1059* (vi), arrows point to the ectopic ALM-PN. For *u1060*, the arrow points to the severely shortened PLM-AN.

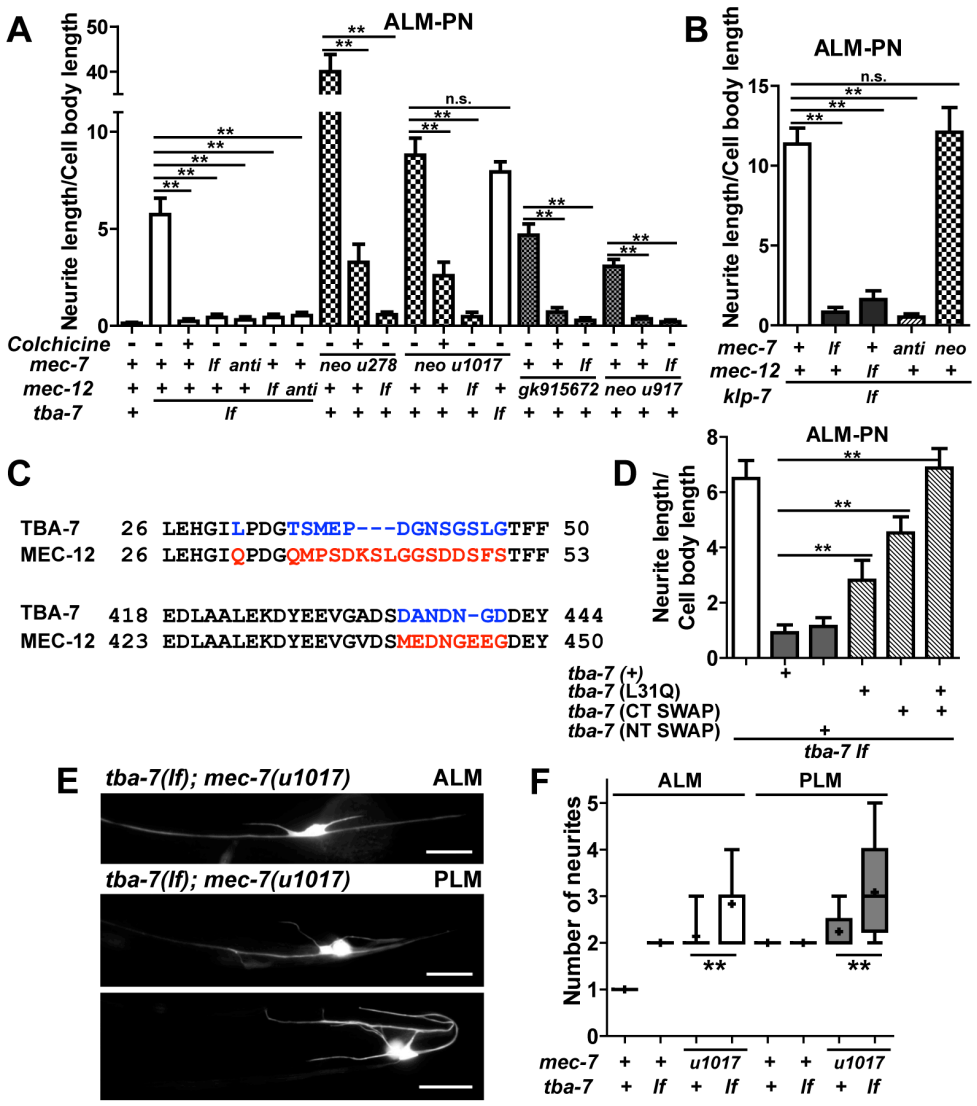

Figure 6. Mutations in *mec-7*, *mec-12*, *tba-7*, and *klp-7* result in the growth of ectopic ALM posterior neurites. (A) The length of ALM-PN in *tba-7(u1015 lf)* and *mec-7* and *mec-12* neomorphic alleles and the effect of 1 mM colchicine and *mec-7(ok2152 lf)*, *mec-7(u957 anti*), *mec-12(tm5083 lf)*, and *mec-12(u1016 anti)* mutations. (B) The length of ALM-PN in *klp-7 lf (tm2143)* mutants and their double mutants with *mec-7(ok2152 lf)*, *mec-7(u957 anti*), *mec-12(tm5083 lf)*, and *mec-7(u1017 neo)*. (C) The differences between the TBA-7 and MEC-12 amino acid sequences in the alignment were labeled in color. (D) The length of ALM-PN in *tba-7(u1015 lf)* carrying the transgene expressing the wild type or mutant TBA-7 proteins. TBA-7 (CT SWAP) had DANDNGD (a.a. 435-441) replaced by MEDNGEEG, TBA-7 (NT SWAP) had TSMEPDGNSGSLG (a.a. 35-47) replaced by QMPSDKSLGGSDDSFS, and TBA-7 (L31Q + CT SWAP) carried both mutations. (E) Sprouting of neurites from the ALM and PLM cell bodies in *tba-7(u1015 lf)*; *mec-7(u1017 neo)* double mutants. (F) The average number of neurites emanating from the cell bodies in *tba-7(u1015 lf)* and *mec-7(u1017 neo)* single mutants and their double mutants.

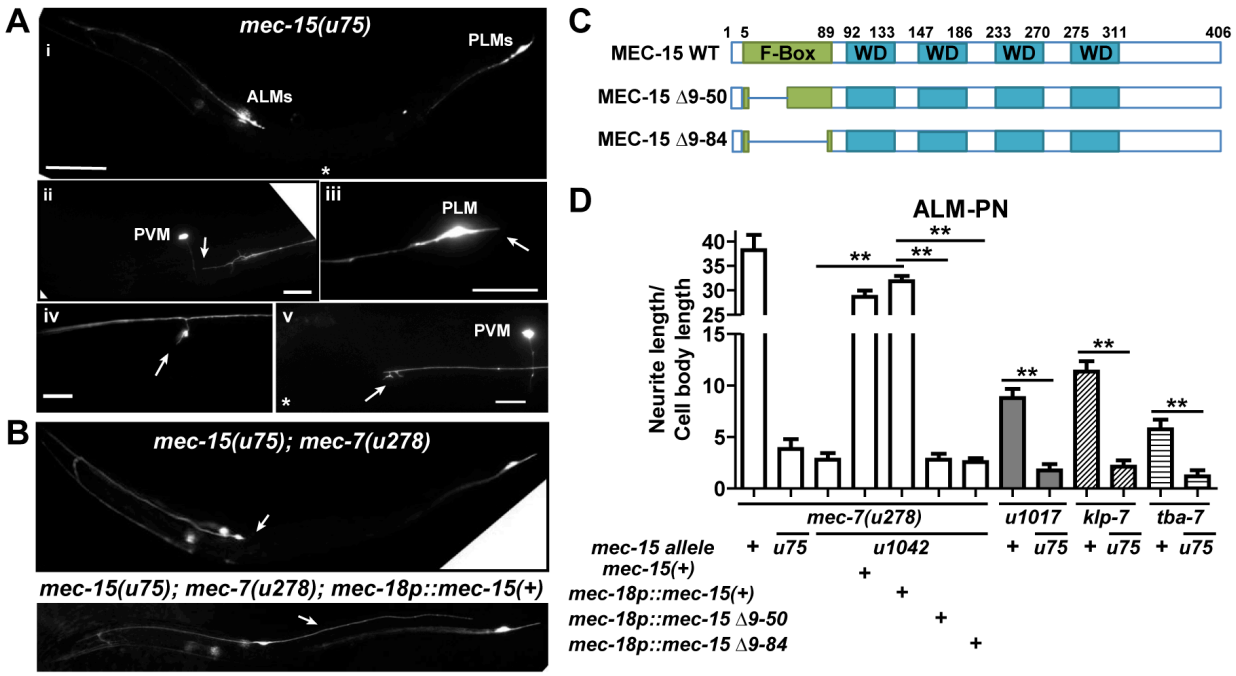

Figure 7. F-box protein MEC-15 promotes neurite growth. (A) TRN morphology in *mec-15(u75 lf)* mutants (i; scale bar = 100 μm). PLM-AN was shortened and did not extend beyond PVM (ii); PLM-PN was also significantly shortened (iii). Synaptic branches of ALM-AN (iv) and PLM-AN (v) could not fully extend in *mec-15* mutants. Scale bar = 20 μm in (ii) through (v). (B) The growth of ALM-PN (arrows) in *mec-7(u278 neo)* mutants was suppressed by *mec-15(lf)* mutations and was restored in the double mutants by expressing wild-type MEC-15 under a TRN-specific *mec-18* promoter. (C) Protein structures of the wild type MEC-15 and F-Box mutants. F-Box and the four WD-40 repeats (WD) were labeled in green and blue, respectively. (D) The length of ALM-PN in various strains. Asterisks indicate significant difference in Tukey-Kramer test.

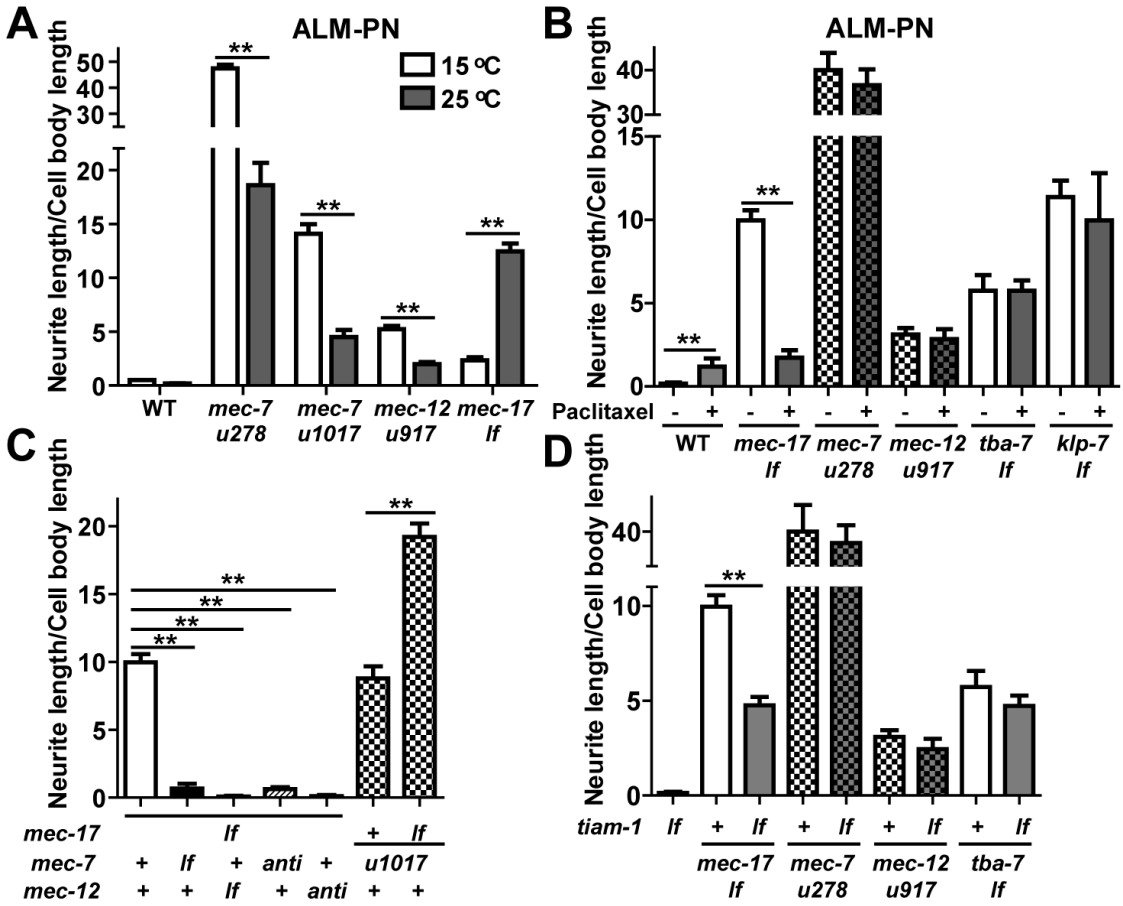

Figure 8. *mec-17 lf* mutations and tubulin *neo* mutations induce the growth of ectopic ALM-PN through different mechanisms. (A) The length of ALM-PN in *mec-17(ok2109 lf)* and tubulin *neo* mutants grown at 15°C and 25°C. Data for the rest of the figure were collected from animals grown at 20°C. (B) The length of ALM-PN in *mec-17(ok2109 lf)*, *mec-7(u278 neo)*, *mec-12(u917 neo)*, *tba-7(u1015 lf)*, and *klp-7(tm2143 lf)* animals treated with or without 100 nM paclitaxel. (C) *mec-17(ok2109 lf)* mutants and their double mutants with *mec-7(ok2152 lf)*, *mec-7(u957 anti*), *mec-12(tm5083 lf)*, *mec-12(u1016 anti)*, and *mec-7(u1017 neo)*. (D) The length of ALM-PN in *mec-17(ok2019 lf)*, *mec-7(u278 neo)*, *mec-12(u917 neo)*, and *tba-7(u1015 lf)* mutants and their double mutants with *tiam-1(u914 lf)*. Asterisks indicate significant difference in Tukey-Kramer test.

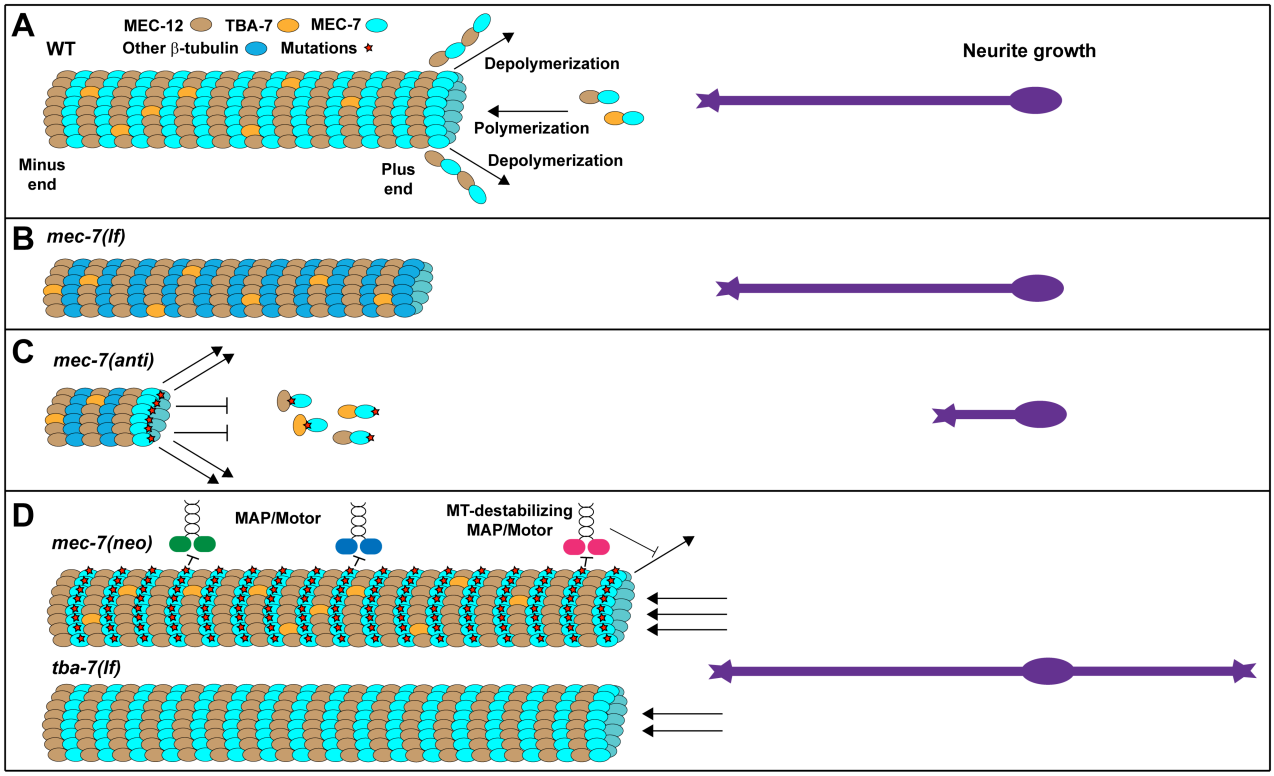

Figure 9. A model for the effect of MT dynamics on neurite development. (A) In wild-type animals, 15-p MTs are mostly made of MEC-12/α-tubulin and MEC-7/β-tubulin. Another α-tubulin TBA-7 is also incorporated into the MTs, probably to increase the dynamics. (B) In the absence of MEC-7, the abundant 15-p MTs are replaced by a few 11-p MTs, which use other β-tubulins for polymerization and can still support neurite growth. Whether those β-tubulins are normally incorporated into the MTs is unclear. (C) *mec-7(anti)* mutations produce dominant-negative MEC-7 proteins with defects in the GTP binding pocket or the intradimer or interdimer interfaces. Such MEC-7 mutants can either sequester all α-tubulin or form toxic heterodimers that can terminate MT elongation upon incorporation. Thus, MT polymerization is blocked and neurite growth is disrupted in *mec-7(anti)* animals. (D) *mec-7(neo)* mutations mostly map to the exterior facing surface of the tubulin structure. When incorporated into the MTs, those MEC-7 mutant proteins may affect the binding of MAPs or motor proteins (e.g. Kinesin 13 family protein KLP-7) by either binding poorer to destabilizing proteins or better to stabilizing proteins. The net result would be hyperstable MTs. The loss of TBA-7 presumably allowed more MEC-12 to be incorporated into the MTs, which led to increased MT stability. Abnormally elevated MT stability caused excessive neurite growth.